Synodic-Resonant Earth/Mars Waypoints

Daniel R. Adamo[1]
Independent Astrodynamics Consultant, Salem, OR 97306

Heliocentric orbits concentric and coplanar with Earth's are placed 19.5% farther from the Sun to naturally maintain a synodic period of 4.27 years, exactly twice that of Mars with Earth. Phasing conditions for infrastructure in these synodic-resonant orbits are developed to minimize propulsive requirements when a 5-day loiter period at this infrastructure is planned during an Earth/Mars transit. With an in-transit loiter, more mass can be transported between Earth and Mars over time than with direct transits if the infrastructure functions as a waypoint to replenish propellant and other consumables while payload is optionally offloaded or supplemented. Four synodic-resonant waypoints cover all Earth/Mars transit opportunities, serve as Earth/Mars communication relays, and offer useful forward/turnaround abort options not available to direct transits. Prospects for constructing a waypoint from known asteroids in nearby orbits are also assessed.

Nomenclature

I_{SP} = propulsive specific impulse (s)
T_S = synodic sequence spanning eight successive Earth/Mars heliocentric oppositions (years)
a = heliocentric orbit semi-major axis (km or AU)
a_E = Earth heliocentric orbit semi-major axis (km or AU)
a_M = Mars heliocentric orbit semi-major axis (km or AU)
a_W = waypoint heliocentric orbit semi-major axis (km or AU)
e = heliocentric orbit eccentricity
g = Earth surface gravity acceleration (km/s^2)
i = heliocentric orbit ecliptic inclination (°)
j = positive integer τ_{EM} resonance multiplier determining ω_W
m_{AA+} = mass immediately after Δv_{AA} completion (kg)
m_{AT-} = mass immediately prior to Δv_{AT} initiation (kg)
m_P = propellant mass (kg)
m_X = maximum permissible $m_Y + m_i + m_P$ (kg)
m_Y = payload mass (kg)
m_i = dry/inert mass (kg)
n = tally of 2LL-compliant Earth/Mars transits during a scan
r_E = geocentric distance (km)
r_M = areocentric distance (km)
t_{Df} = Leg-A or C departure window close epoch for 2LL processing (UTC date)
t_{Di} = Leg-A or C departure window open epoch for 2LL processing (UTC date)
v_{EX} = propulsive exhaust speed (km/s)
v_∞ = asymptotic speed (km/s)

[1] Sole Proprietor, 8119 Kloshe Ct. S, adamod@earthlink.net, and AIAA Associate Fellow

$v_{\infty Aarr}$ = Leg-A arrival waypoint-centered asymptotic speed (km/s)
$v_{\infty Adep}$ = Leg-A departure geocentric asymptotic speed (km/s)
$v_{\infty Barr}$ = Leg-B arrival Mars-centered asymptotic speed (km/s)
$v_{\infty Bdep}$ = Leg-B departure waypoint-centered asymptotic speed (km/s)
$v_{\infty Carr}$ = Leg-C arrival waypoint-centered asymptotic speed (km/s)
$v_{\infty Cdep}$ = Leg-C departure Mars-centered asymptotic speed (km/s)
$v_{\infty Darr}$ = Leg-D arrival Earth-centered asymptotic speed (km/s)
$v_{\infty Ddep}$ = Leg-D departure waypoint-centered asymptotic speed (km/s)
$v_{\infty arr}$ = v_∞ of a generic interplanetary arrival (km/s)
$v_{\infty dep}$ = v_∞ of a generic interplanetary departure (km/s)
$v_{\infty depMax}$ = maximum permissible $v_{\infty Adep}$, $v_{\infty Bdep}$, $v_{\infty Cdep}$, or $v_{\infty Ddep}$ for 2LL processing(km/s)
Υ = the first point of Aries at which λ is zero
ΔT = the interval by which 2LL increments trajectory segment departure/arrival epochs (days)
Δt = total Earth/Mars transit time, including OLP or RLP (days)
Δt_{Lmin} = minimum permissible OLP or RLP for 2LL processing (days)
Δt_{Max} = maximum permissible Δt for 2LL processing (days)
Δv = change-in-velocity magnitude (km/s)
Δv_{AA} = Δv required to complete a turnaround abort upon return to the original departure location (km/s)
Δv_{AT} = Δv required to initiate a turnaround abort after an interplanetary departure (km/s)
Δv_E = Δv required to depart from or arrive at Earth (km/s)
Δv_M = Δv required to depart from or arrive at Mars (km/s)
$\Delta\lambda$ = change in λ (°)
$\sum v_\infty$ = $v_{\infty Adep} + v_{\infty Aarr} + v_{\infty Bdep} + v_{\infty Barr}$ or $v_{\infty Cdep} + v_{\infty Carr} + v_{\infty Ddep} + v_{\infty Darr}$ (km/s)
$\sum v_{\infty Max}$ = maximum permissible $\sum v_\infty$ for 2LL processing (km/s)
ε = geocentric Sun-Earth-Mars elongation angle (°)
ε' = areocentric Sun-Mars-Earth elongation angle (°)
λ = heliocentric ecliptic longitude (°)
λ_{31} = a Leg-AB waypoint's λ at the Earth/Mars heliocentric opposition epoch in year 2031 (°)
λ_{31r} = a Leg-CD waypoint's λ at the Earth/Mars heliocentric opposition epoch in year 2031 (°)
λ_{33} = a Leg-AB waypoint's λ at the Earth/Mars heliocentric opposition epoch in year 2033 (°)
λ_{33r} = a Leg-CD waypoint's λ at the Earth/Mars heliocentric opposition epoch in year 2033 (°)
μ_E = Earth reduced mass (km^3/s^2)
μ_M = Mars reduced mass (km^3/s^2)
μ_S = Sun reduced mass (km^3/s^2)
τ_{EM} = Earth/Mars heliocentric synodic period (s, days, or months)
ω_E = Earth heliocentric position vector mean angular rate (rad/s)
ω_M = Mars heliocentric position vector mean angular rate (rad/s)
ω_W = waypoint heliocentric position vector mean angular rate (rad/s)

1.0 Introduction

This paper documents the concept of synodic-resonant waypoints in the context of two-leg human transits between Earth and Mars. In an outbound transit, Leg-A departs Earth and arrives at the waypoint. Following an outbound loiter period (OLP), Leg-B departs the waypoint and

arrives at Mars. In a return transit, Leg-C departs from Mars and arrives at the waypoint. Following a return loiter period (RLP), Leg-D departs the waypoint and arrives at Earth.

In these two-leg transits, a waypoint's heliocentric trajectory is distinct from that of an Earth/Mars cycler [1] because the latter facilitates single-leg or nonstop transits by crossing the two planets' orbits. Heliocentric waypoint orbits considered in this initial study are nearly concentric and coplanar with Earth's. Thus, waypoint orbits have near-zero eccentricity, while cyclers must have eccentricity greater than 0.16 to cross the orbits of Earth and Mars.

The utility of any waypoint or cycler is heavily dependent on the frequency with which it is positioned for reuse. Suitable waypoint and cycler infrastructure is massive to provide a spacious radiation-shielded habitat for humans and cached consumables such as propellant for visiting vehicles carrying those humans. Consequently, a trade-off can arise between maximizing waypoint/cycler reuse frequency and maintaining that frequency with minimal propulsion.

As will be demonstrated, waypoints in orbits resonating with the Earth/Mars synodic period are available for reuse every two such periods, approximately once every 4.27 years, with virtually zero propulsion. Subsequent sections will determine how a waypoint should be phased in its orbit such that visiting vehicle propulsive requirements are minimized during outbound or return transits. To examine what reservoir of natural waypoint prospects may exist, a survey of known near-Earth objects (NEOs) in the Amor group[2] is provided.

Waypoints, in their easily maintained orbits, serve Earth/Mars human transits in multiple capacities. First, they function as interplanetary rest stops, permitting consumable loads aboard transit vehicles to be replenished, and thereby increasing deliverable payload mass over time with respect to single-leg transit designs and cyclers. Consumables on NEO waypoints may be obtained from in situ resources, or they may be accumulated from resource-rich objects in the Amor group and more remote small bodies. Second, waypoints can serve as communications relay stations between Earth and Mars when the two planets are on opposite sides of the Solar System and the Sun would otherwise interfere with transmissions. Third, waypoints become an optional post-abort haven when vehicle malfunctions or hazards such as solar radiation outbursts preclude flying a transit as planned.

2.0 Earth/Mars Orbit Period Resonance

The heliocentric mean semi-major axes for Earth and Mars are a_E = 149598023 km and a_M = 227939186 km, respectively [2, Table 15.6, p. 704]. With the Sun's reduced mass μ_S = 132712440041.93938 km^3/s^2 [3, object code 10], Kepler's third law relates these semi-major axes to the planets' mean anomaly rates, the mean angular rates of their heliocentric position vectors.

$$\omega_E = \sqrt{\mu_S / a_E^3} = 1.99098\text{E-}07 \text{ rad/s} \quad (1)$$

[2] Reference https://cneos.jpl.nasa.gov/about/neo_groups.html for NEO orbit group definitions (accessed 4 January 2024).

$$\omega_M = \sqrt{\mu_S / a_M^3} = 1.05859\text{E-}07 \text{ rad/s} \quad (2)$$

Suppose Mars is in opposition with Earth such that the two planets have the same ecliptic longitude λ.[3] The synodic period τ_{EM} is the average time interval until the next Earth/Mars opposition and is computed as a positive interval using Equation 3.

$$\tau_{EM}(\omega_E - \omega_M) = 2\pi \longrightarrow \tau_{EM} = \frac{2\pi}{\omega_E - \omega_M} = 67387826 \text{ s} \quad (3)$$

The value for τ_{EM}, equivalent to 780.0 days or 26 months, gives rise to the average interval between successive opportunities for single-leg transits between Earth and Mars. When using high-thrust propulsion for human transport, practical departures from Earth or Mars typically arise during the months immediately before opposition.

Because τ_{EM} is two months longer than two Earth years, opposition locations with Mars advance in inertial space around Earth's heliocentric orbit by an average near $360 \times 2/12 = 60°$ in λ per τ_{EM}. This advance is not uniform because the heliocentric orbit eccentricity of Mars is 0.0934, a value 5.6 times that of Earth's orbit [2, Table 15.6, p. 704]. Mars eccentricity imposes appreciable deviations in heliocentric position from those inferred from ω_M over time.

Table 1 illustrates a progression of Earth/Mars oppositions very nearly circuiting 360° in λ as inferred from UTC date. When reckoned for Earth's northern hemisphere seasons, λ is zero at the Vernal Equinox in March, 90° at the Summer Solstice in June, 180° at the Autumnal Equinox in September, and 270° at the Winter Solstice in December. The eight oppositions in Table 1 comprise a synodic sequence T_S requiring 17 days less than 15.0 Earth years to complete. Meanwhile, the orbit of Mars has swept out a heliocentric angle of $5462.3 \times 86400\omega_M$ = 49.9594 radians, equivalent to 7.9513 Mars years. The orbits of Mars and Earth therefore have a period resonance very near 8 : 15.

Table 1. Eight successive Earth/Mars opposition dates define seven τ_{EM} intervals spanning one synodic sequence T_S in Phase Elapsed Time (PET) reckoned from the first opposition's UTC date.

Opposition UTC Date	Earth/Mars Dist. (10^6 km)	PET (days)	ΔPET (days)
04.497 May 2031	83.609	0.0	
28.057 Jun 2033	63.913	785.6	785.6
15.813 Sep 2035	57.101	1595.3	809.7
19.377 Nov 2037	74.739	2390.9	795.6
02.639 Jan 2040	91.799	3165.1	774.2
06.198 Feb 2042	100.514	3931.0	765.9
11.530 Mar 2044	99.917	4695.0	764.0
17.749 Apr 2046	89.938	5462.3	767.3

[3] Ecliptic longitude is measured in the ecliptic plane (that of Earth's heliocentric orbit), increasing in the direction of Earth's heliocentric motion from zero at the first point of Aries (♈).

The average of Table 1's seven ΔPET values is 780.3 days, in close agreement with the mean value computed from Equation 3. A ΔPET value tends to be greater than 780 days to the degree Mars is nearer perihelion (when the corresponding Earth/Mars distance is less). The closest Earth/Mars oppositions are called *perihelic* and will always fall in late August or early September until the line of apsides in the heliocentric orbit of Mars shifts significantly in λ many millennia in the future.

3.0 Earth/Mars Synodic-Resonant Waypoint Orbits

The synodic period τ_{EM} defines average time required to reproduce a specified Sun-Earth-Mars elongation angle ε. A waypoint orbit is sought whose heliocentric mean anomaly rate ω_W produces a synodic-resonant period $j\,\tau_{EM}$ with Earth and Mars, where j is a positive integer. The associated synodic resonance constraint is then obtained from Equation 4.

$$j\tau_{EM} = \frac{j2\pi}{\omega_E - \omega_M} = \frac{2\pi}{\omega_E - \omega_W} \rightarrow \omega_W = \omega_E - \frac{\omega_E - \omega_M}{j} \tag{4}$$

With synodic period $j\,\tau_{EM}$, waypoint availability is highest for the smallest practical j. Using $j = 1$ in Equation 4 produces the trivial result $\omega_W = \omega_M$, a not very useful waypoint whose circular orbit crosses that of Mars at its mean distance from the Sun a_M. The $j = 1$ resonance orbit therefore resembles that of a cycler more than a waypoint. At $j = 2$, however, a desirable value intermediate with respect to ω_M and ω_E is obtained such that ω_W = 1.52478E-07 rad/s. Equation 1 is then adapted to solve for the $j = 2$ waypoint orbit's semi-major axis.

$$a_W = \sqrt[3]{\frac{\mu_S}{\omega_W^2}} = 178716582\ \text{km} = 1.19464656\ \text{AU} \tag{5}$$

The $j = 2$ intermediate waypoint orbit is therefore the focus of this paper. This orbit lies about 19.5% beyond Earth's heliocentric distance (Mars lies an average of 52% beyond Earth's heliocentric distance) and is naturally repositioned with respect to a specified Sun-Earth-Mars ε every two τ_{EM}, an average availability interval of 4.27 years.

Other synodic resonances exist naturally throughout the Solar System. One between the Earth, Mars, and dwarf planet 1 Ceres is documented by Borisov [4], along with further examples.

To illustrate $j = 2$ waypoint dynamics, consider an example whose waypoint and Mars are in opposition with Earth at 4.497 May 2031 UTC. Figure 1 plots the ecliptic longitude λ of the Earth, Mars, and waypoint from before this epoch until after the opposition at 15.813 September 2035 UTC, spanning a full waypoint synodic period. Data in Figure 1 are obtained from JPL's *Horizons* ephemeris server [3] with the waypoint orbit defined as a user-specified small body (USSB) having zero mass and subject only to gravitational accelerations.

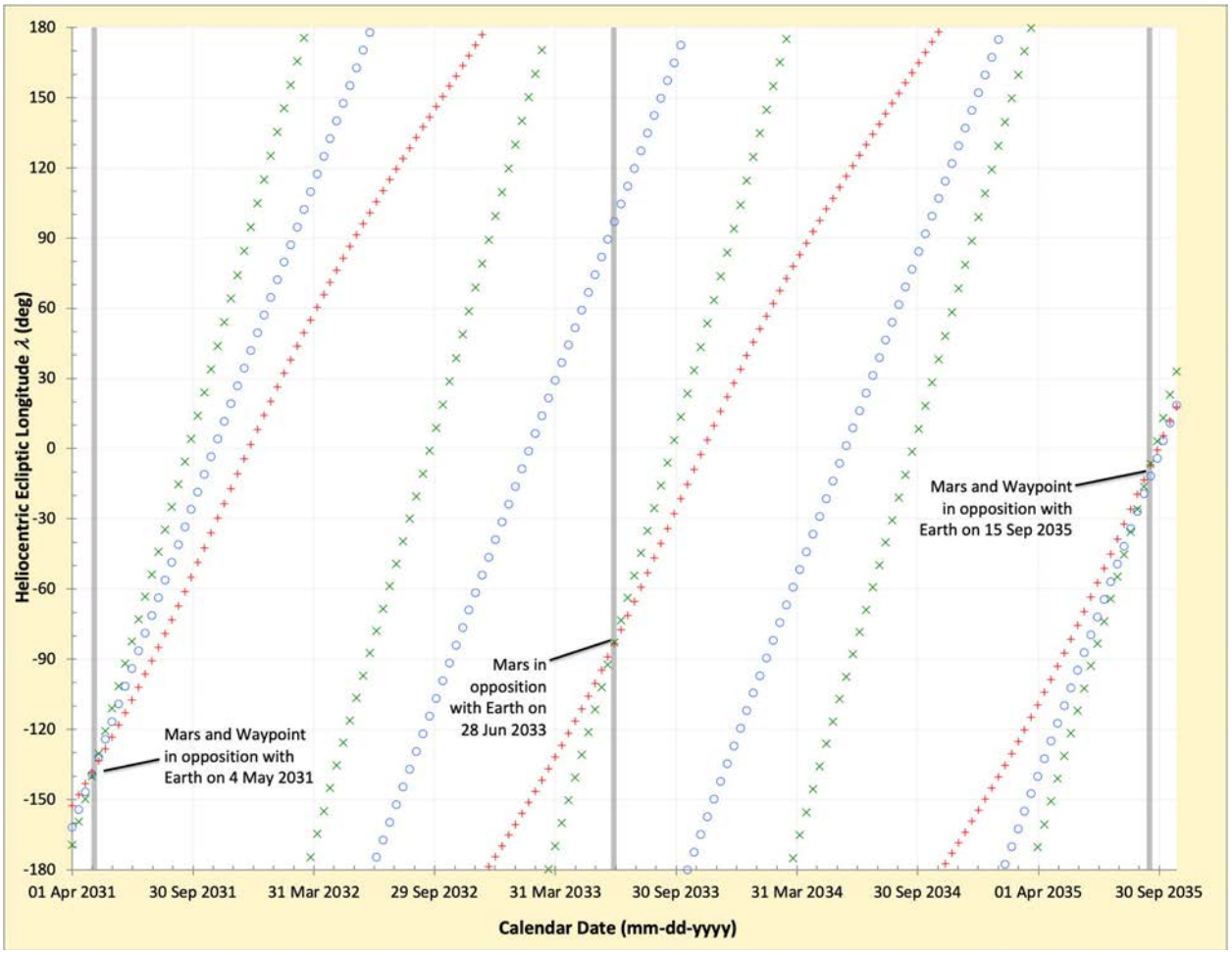

Figure 1. Heliocentric ecliptic longitude λ is plotted as a function of time every 10 days for Earth (x markers), Mars (+ markers), and a $j = 2$ synodic-resonant waypoint with these two planets (o markers). Mars is in opposition with Earth at times indicated by vertical gray lines.

Note the nonlinearity with time among Figure 1's + Mars markers. This is due to elevated eccentricity in the heliocentric orbit of Mars with respect to the nearly circular orbits of Earth and the waypoint. As expected, the steepest slope among Mars markers is around the time of perihelion, and Mars oppositions with Earth advance through Mars perihelion in Figure 1. Thus, the 15 September 2035 opposition is the closest Earth comes to Mars during the time spanned by Figure 1 and Table 1.

Because its orbit is initialized in opposition with Earth on 4 May 2031, the Figure 1 waypoint's $j = 2$ synodic resonance ensures it is also nearly in opposition with Earth on 15 September 2035, two Earth/Mars oppositions later. At the intervening Mars opposition with Earth on 28.057 June 2033 UTC, the waypoint is on the opposite side of the Solar System from the two planets, 180° in λ away from them. Other $j = 2$ synodic-resonant waypoint orbits can be initialized to exhibit nearly constant non-zero λ bias with respect to the Earth-Mars line when Mars is in opposition with Earth. Theoretical waypoint orbits with biases useful in Earth/Mars transits are documented in Sections 5.0 and 6.0.

Despite the many gravitational perturbations modeled by *Horizons* in a USSB ephemeris and variations from Mars orbit eccentricity, the Figure 1 waypoint orbit maintains a high degree of synodic resonance at $j = 2$ during Table 1's oppositions. Table 2 quantifies this resonance with $\Delta\lambda$, a difference reckoned in the sense "waypoint λ minus Earth/Mars λ" when the two planets are in opposition. Thus, a positive $\Delta\lambda$ indicates the waypoint is ahead of Earth and Mars in their heliocentric orbits.

Table 2. The degree to which Figure 1's waypoint $j = 2$ orbit is in synodic resonance with Earth and Mars is quantified by $\Delta\lambda$. In the absence of relatively minor orbit perturbations and appreciable Mars orbit eccentricity, $\Delta\lambda$ would alternate between zero and ±180° at each Earth/Mars opposition date.

Opposition UTC Date	Earth/Mars λ (deg)	$\Delta\lambda$ (deg)
04.497 May 2031	-136.592	0.000
28.057 Jun 2033	-83.770	-179.918
15.813 Sep 2035	-7.694	-4.831
19.377 Nov 2037	+56.849	+171.075
02.639 Jan 2040	+101.278	-8.936
06.198 Feb 2042	+137.238	+173.126
11.530 Mar 2044	+170.979	-3.910
17.749 Apr 2046	-152.748	+178.867

Table 2 demonstrates simulated waypoints can be configured as USSB ephemerides resonating with Earth/Mars synodic motion to a precision of about 10° in λ over a period of decades.

4.0 Two-Leg Lambert Scanner (2LL) Overview

Like NASA's Near-Earth Object Human Space Flight Accessible Targets Study processor (NHATS, pronounced "gnats"), 2LL computations are based on the method of embedded trajectory grids [5, p. 7]. In this algorithm, a Leg-A/C heliocentric Lambert trajectory solution is first assessed against preliminary compliancy criteria. If these criteria are satisfied, Leg-A/C waypoint arrival conditions (together with an OLP/RLP delay) spawn multiple Leg-B/D heliocentric Lambert trajectory solutions for final compliancy assessments. Only transits satisfying all compliancy criteria are reported in 2LL output.

Compliancy criteria for 2LL are summarized in Table 3. The final Table 3 asymptotic speed summation $\sum v_\infty$ criterion is particularly distinct from NHATS to avoid specifying Earth-specific assumptions such as parking orbit and atmospheric entry heights. In addition to the $\sum v_\infty$ criterion, 2LL makes a major departure from NHATS by lifting the Earth roundtrip constraint.

Along with Table 3 compliancy criteria, the tally of compliant 2LL transits n is dependent on the interval ΔT by which any leg's departure/arrival time and the associated waypoint loiter period are incremented. A notional $\Delta T = 5$ days (NHATS uses 8 days) applies to all 2LL scans documented herein.

Table 3. An "x" appears in columns designating trajectory legs to which a 2LL compliancy criterion is applied. Satisfying preliminary Leg-A/C criteria is necessary, but not sufficient, for a two-leg transit to also satisfy Leg-B/D criteria and appear in 2LL output.

Criterion	Leg-A/C	Leg-B/D
Leg-A/C departure on or after epoch t_{Di} and on or before epoch t_{Df}	x	
OLP/RLP $\geq \Delta t_{Lmin}$		x
Two-leg transit time $\Delta t = \Delta t_{A/C}$ + OLP/RLP + $\Delta t_{B/D} \leq \Delta t_{Max}$	x	x
Asymptotic departure speed $v_{\infty A/B/C/Ddep} < v_{\infty depMax}$	x	x
The sum $\sum v_\infty = v_{\infty A/Cdep} + v_{\infty A/Carr} + v_{\infty B/Ddep} + v_{\infty B/Darr} < \sum v_{\infty Max}$	x	x

Output from 2LL is of two types. Color-coded icicle plot graphics[4] are produced over the Leg-A/C departure interval t_{Di} to t_{Df} with the primary dependent variable being two-leg transit time Δt including OLP/RLP (see Figures 3 and 5 for examples). The secondary dependent variable in an icicle plot is color-coded regions pertaining to either $\sum v_\infty$ or OLP/RLP.

The second type of 2LL output is text-based and relates parametric values specific to three transits among the n determined to be compliant. First among these has minimum $\sum v_\infty$, and it is accompanied by transits with minimum Δt and maximum OLP/RLP.

To quantify trades between conventional direct Earth/Mars transits and two-leg transits through a waypoint, 2LL supports an optional single-leg processing mode. An OLP/RLP does not pertain to single-leg transits, so 2LL output for these scans only includes a $\sum v_\infty$ icicle plot, together with parameters from the minimum $\sum v_\infty$ and minimum Δt transits.

5.0 Earth-To-Mars Outbound Waypoint Phasing Assessments

The parameter used to obtain notionally optimal outbound phasing in support of Earth-waypoint-Mars transits is waypoint ecliptic longitude λ_{31} at the Table 1 Earth/Mars opposition epoch 04.497 May 2031 UTC. With λ_{31} = -136.592° when Earth and Mars are in opposition at this epoch (per Table 2), the waypoint is also in opposition with Earth and mimics Figure 1's example. Under λ_{31}= -136.592° geometry, a two-leg transit tends to be over-phased in λ throughout. Ideally, Mars should lead the waypoint (with more positive λ) and the waypoint should in turn lead Earth at Earth departure. Consequently, a series of 2LL scans in the 2031 Earth/Mars opposition timeframe is performed, each scan with a specific λ_{31} and the following 2LL control values shared among them.

1) t_{Di} = 1.0 Nov 2030 UTC
2) t_{Df} = 1.0 May 2031 UTC
3) Δt_{Lmin} = 5.0 days
4) Δt_{Max} = 300.0 days
5) $v_{\infty depMax}$ = 8.0 km/s[5]

[4] These graphics are named for the icicle-shaped regions of compliant missions in NHATS processing over 26-year Earth departure intervals. In the context of 2LL 's Earth/Mars transit processing, these intervals are only about 6 months, making for very broad "icicles" in this paper's illustrations.

[5] This liberal limit's primary purpose is to quickly exclude "wrong way" retrograde heliocentric trajectories from 2LL mission compliance.

6) $\sum v_{\infty Max}$ = 20.0 km/s

For comparison, a single-leg 2LL scan is made with these control values as well (the Δt_{Lmin} control being irrelevant). Results from these scans are recorded in Table 4 and focus on the minimal $\sum v_\infty$ compliant transit as the subjective criterion for an optimal λ_{31}.

Table 4. The rightmost two columns apply to the 2LL-compliant transit with minimum $\sum v_\infty$ among *n* others tallied by each λ_{31}-specific scan in the 2031 Earth/Mars opposition timeframe. The single-leg scan has no waypoint and is thus independent of λ_{31}.

λ_{31} (deg)	*n*	$\sum v_\infty$ (km/s)	Δt (days)
Single-leg	1052	6.747	285.0
-136.592	1958	17.905	300.0
-146.592	66409	11.499	300.0
-156.592	104840	9.480	300.0
-166.592	33276	14.932	300.0
-176.592	0		

Each of the two-leg scans in Table 4 is associated with a minimum $\sum v_\infty$ transit whose OLP is the minimally compliant 5.0 days. All Table 4 two-leg scans also have Δt = 300.0 days because minimum $\sum v_\infty$ will generally be limited by the imposed Δt_{Max} value in this paper. Owing to its maximum *n* and minimum $\sum v_\infty$ among other two-leg scans in Table 4, λ_{31} = -156.592° is selected as optimal for waypoint phasing in Earth-to-Mars transits beginning with the 2031 opposition's timeframe.

For each "viable" opposition in Table 2 (namely those four with nearly zero $\Delta\lambda$), a 2LL scan is made with its waypoint coasted as a USSB from λ_{31} = -156.592° initial conditions. Each of these is supplemented by a single-leg scan with the same control values for comparison purposes. Furthermore, all 2LL control values are held at those previously given except for the six-month Leg-A departure interval from t_{Di} to t_{Df}. This interval slips to end near the Earth/Mars opposition epoch being assessed. Results of the four 2LL scans, together with their single-leg counterparts, are summarized in Table 5 for transits with minimal $\sum v_\infty$ in the viable Leg-A departure intervals.

When generalized to other than minimum $\sum v_\infty$ transits, Table 5 data indicate Leg-A/B transits incur greater $\sum v_\infty$ and Δt than do single-leg transits in the same timeframe. However, as documented in subsequent sections, other factors such as deliverable payload mass and abort options favor waypoint-supported transits.

Table 5. The rightmost two columns apply to the 2LL -compliant transit with minimum $\sum v_\infty$ among n others tallied by each scan in the corresponding Earth/Mars opposition timeframe. Sums in the Δt column correspond to Leg-A + OLP + Leg-B durations. A single-leg scan has no waypoint and is thus independent of λ_{31}.

t_{Di} to t_{Df} UTC Dates	2LL Scan Mode	n	$\sum v_\infty$ (km/s)	Δt (days)
1.0 Nov 2030 to 1.0 May 2031	Single-leg	1052	6.747	285
	λ_{31} = -156.592°	104840	9.480	145 + 5 + 150 = 300
1.0 Mar 2035 to 1.0 Sep 2035	Single-leg	1292	5.855	200
	λ_{31} = -156.592°	48026	13.797	120 + 5 + 175 = 300
1.0 Juy 2039 to 1.0 Jan 2040	Single-leg	717	7.206	300
	λ_{31} = -156.592°	15851	15.044	120 + 5 + 175 = 300
1.0 Sep 2043 to 1.0 Mar 2044	Single-leg	834	5.811	300
	λ_{31} = -156.592°	35931	12.545	125 + 5 + 170 = 300

The Table 4 transit with minimum $\sum v_\infty$ whose waypoint orbit is initialized at λ_{31} = -156.592° has its itinerary summarized in Table 6 and its heliocentric motion plotted in Figure 2. From the 2LL scan giving rise to this minimum $\sum v_\infty$ transit, the Figure 3 icicle plot is obtained.

Table 6. The following itinerary has a minimal $\sum v_\infty$ = 9.480 km/s among the n = 104840 2LL -compliant Leg-A/B transits departing Earth from 1.0 Nov 2030 to 1.0 May 2031 UTC. The associated waypoint is initialized at λ_{31} = -156.592°. Phase Elapsed Time (PET) is reckoned from the Earth departure UTC date.

UTC Date	PET (d)	Event
16.0 Dec 2030	000.0	Leg-A Earth departure: v_∞ = 2.331 km/s
10.0 May 2031	145.0	Leg-A waypoint arrival: v_∞ = 1.775 km/s
15.0 May 2031	150.0	Leg-B waypoint departure: v_∞ = 1.919 km/s
12.0 Oct 2031	300.0	Leg-B Mars arrival: v_∞ = 3.455 km/s

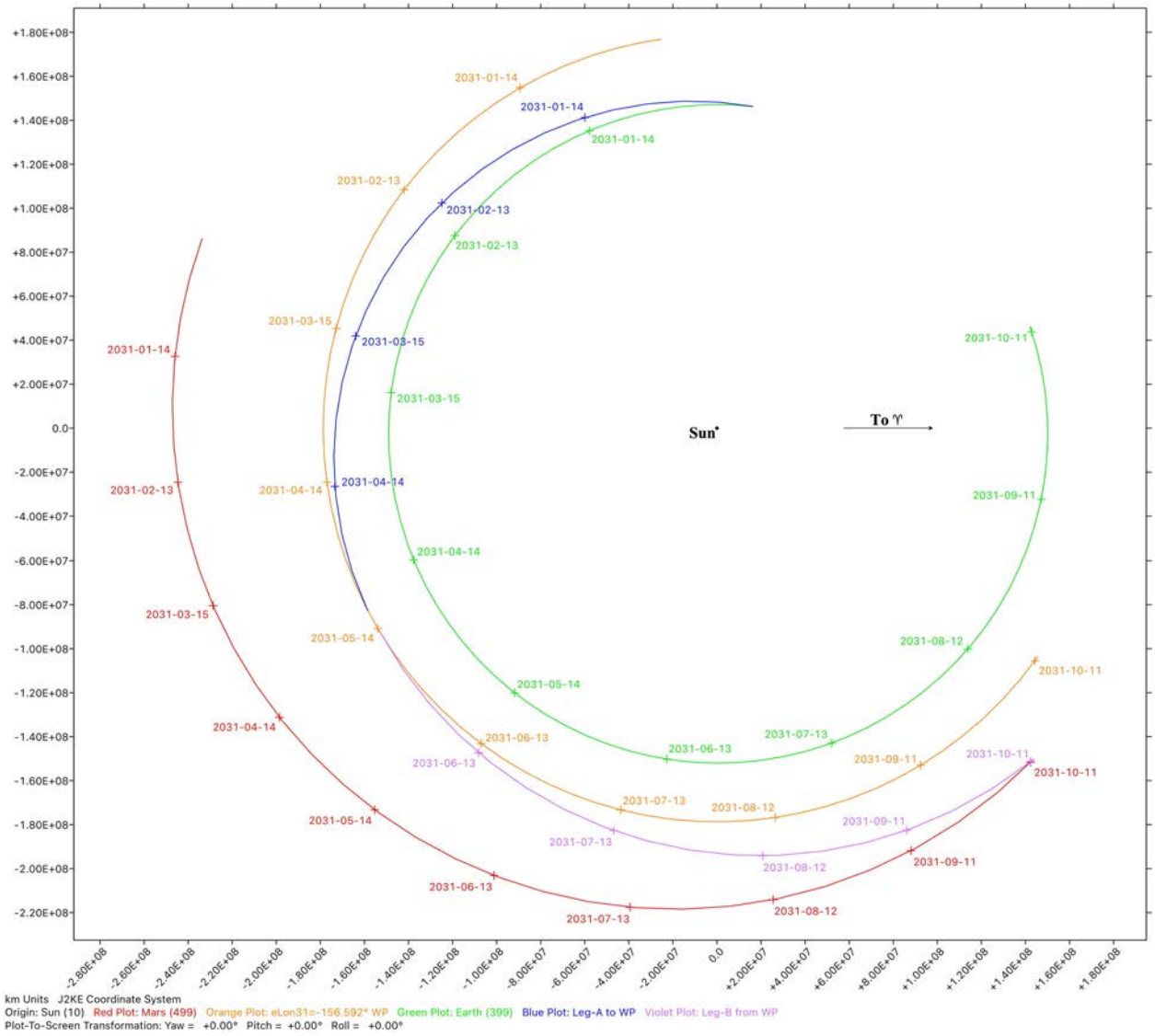

Figure 2. Inertial heliocentric ecliptic plane motion of the Earth (green), waypoint (orange), and Mars (red) is accompanied by Leg-A (blue) and Leg-B (violet) from the Table 6 transit itinerary. Time ticks ("+" markers) are annotated with 00:00 UTC dates in YYYY-MM-DD format at 30-day intervals. The direction annotated "To ♈" points along zero ecliptic longitude λ.

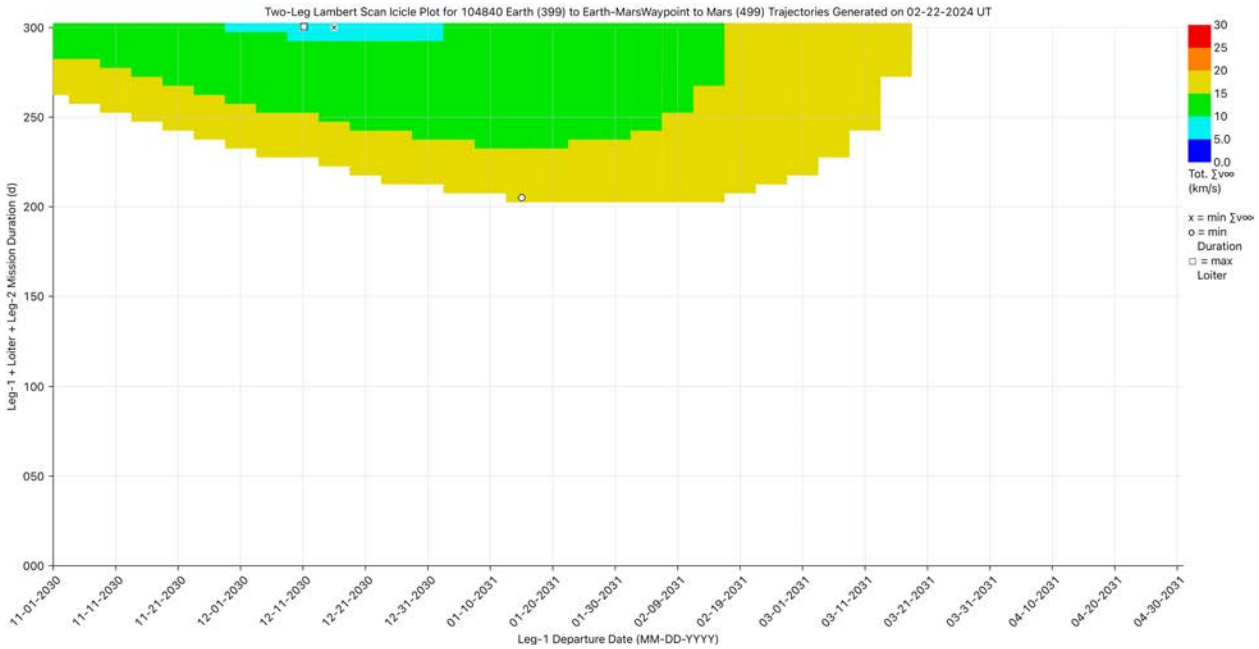

Figure 3. In this icicle plot, Leg A/B transit duration Δt is plotted against Earth departure date t_D and colored according to $\sum v_\infty$ as defined in the legend at upper right. The transit with minimum $\sum v_\infty$, detailed in Table 6 and Figure 2, is annotated by the black "x" marker at top left.

Outbound transits associated with Table 2 opposition periods beginning in 2031 having $\Delta\lambda$ near zero are serviced by a waypoint orbit initialized at λ_{31} = -156.592°. Can a λ_{33} waypoint orbit initialization be developed for interleaved oppositions beginning in 2033? To do so, retain all the 2LL control values adopted for λ_{31} development except for the first two defining the Earth departure interval. These are modified as follows.

1) t_{Di} = 1.0 Jan 2033 UTC
2) t_{Df} = 1.0 Juy 2033 UTC

A single-leg 2LL scan is made with these control values as well. Results from λ_{33} scans are recorded in Table 7 and focus on the minimal $\sum v_\infty$ compliant transit as the subjective criterion for an optimal λ_{33}.

Table 7. The rightmost two columns apply to the 2LL -compliant transit with minimum $\sum v_\infty$ among *n* others tallied by each λ_{33}-specific scan in the 2033 Earth/Mars opposition timeframe. The single-leg scan has no waypoint and is thus independent of λ_{33}.

λ_{33} (deg)	*n*	$\sum v_\infty$ (km/s)	Δt (days)
Single-leg	1254	6.336	200
-83.770	45442	13.591	300
-93.770	175633	7.729	300
-103.770	128212	10.131	300
-113.770	6644	16.224	300
-123.770	0		

Each of the two-leg scans in Table 7 is associated with a minimum $\sum v_\infty$ transit whose OLP is the minimally compliant 5.0 days. Owing to its maximum n and minimum $\sum v_\infty$ among other two-leg scans in Table 7, λ_{33} = -93.770° is selected as optimal for waypoint phasing in Earth-to-Mars transits beginning with the 2033 opposition's timeframe.

For each "viable" opposition in Table 2 (namely those four with nearly ±180° $\Delta\lambda$), a 2LL scan is made with its waypoint coasted as a USSB from λ_{33} = -93.770° initial conditions. Each of these is supplemented by a single-leg scan with the same control values for comparison purposes. Furthermore, all 2LL control values are held at those previously given except for the six-month Leg-A departure interval ending at the approximate Earth/Mars opposition epoch being assessed. These intervals are summarized in Table 8.

Table 8. Leg-A Earth departure intervals are given for λ_{33} = -93.770° waypoint 2LL scans spanning viable Table 2 Earth-to-Mars transit opportunities. The Earth/Mars opposition date near close of each window is included for context.

t_{Di} UTC Date	t_{Df} UTC Date	Opposition UTC Date
1.0 Jan 2033	1.0 Juy 2033	28.057 Jun 2033
1.0 Jun 2037	1.0 Dec 2037	19.377 Nov 2037
1.0 Aug 2041	1.0 Feb 2042	06.198 Feb 2042
1.0 Nov 2045	1.0 May 2046	17.749 Apr 2046

Results of the four 2LL scans, together with their single-leg counterparts, are summarized in Table 9 for transits with minimal $\sum v_\infty$ in the viable Leg-A departure intervals. Table 9 two-leg transit results appear equally viable compared to intervening transits appearing in Table 5.

Table 9. The rightmost two columns apply to the 2LL -compliant transit with minimum $\sum v_\infty$ among n others tallied by each scan in the corresponding Earth/Mars opposition timeframe. Sums in the Δt column correspond to Leg-A + OLP + Leg-B durations. A single-leg scan has no waypoint and is thus independent of λ_{33}.

t_{Di} to t_{Df} UTC Dates	2LL Scan Mode	n	$\sum v_\infty$ (km/s)	Δt (days)
1.0 Jan 2033 to 1.0 Juy 2033	Single-leg	1254	6.336	200
	λ_{33} = -93.770°	175633	7.729	145 + 5 + 150 = 300
1.0 Jun 2037 to 1.0 Dec 2037	Single-leg	857	7.013	220
	λ_{33} = -93.770°	49233	11.318	125 + 5 + 170 = 300
1.0 Aug 2041 to 1.0 Feb 2042	Single-leg	740	5.772	300
	λ_{33} = -93.770°	17674	13.985	115 + 5 + 180 = 300
1.0 Nov 2045 to 1.0 May 2046	Single-leg	948	6.416	290
	λ_{33} = -93.770°	39429	12.545	130 + 5 + 165 = 300

It should be no surprise that the difference λ_{33} - λ_{31} = -93.770 - (-156.592) = +62.822° is near +60°. Successive Earth/Mars oppositions advance in ecliptic longitude by an average of +60° as documented in Section 2.0.

6.0 Mars-To-Earth Return Waypoint Phasing Assessments

The parameter used to obtain notionally optimal phasing in support of return Mars-waypoint-Earth transits is waypoint ecliptic longitude λ_{31r} at the Table 1 Earth/Mars opposition epoch 04.497 May 2031 UTC. With λ_{31r} = -136.592° when Earth and Mars are in opposition at this epoch (per Table 2), the waypoint is also in opposition with Earth. Under λ_{31r} = -136.592° geometry, a two-leg transit tends to be under-phased in λ throughout. Ideally, Mars should lead the waypoint (with more positive λ) and the waypoint should in turn lead Earth at Mars departure. Consequently, a series of 2LL scans in the 2031 Earth/Mars opposition timeframe are performed, each with a specific λ_{31r} and the following 2LL control values shared among them. These are the same values previously used to optimize Earth-waypoint-Mars phasing and are repeated here as a convenience to readers.

1) t_{Di} = 1.0 Nov 2030 UTC
2) t_{Df} = 1.0 May 2031 UTC
3) Δt_{Lmin} = 5.0 days
4) Δt_{Max} = 300.0 days
5) $v_{\infty depMax}$ = 8.0 km/s[6]
6) $\sum v_{\infty Max}$ = 20.0 km/s

For comparison, a single-leg 2LL scan is made with these control values as well. Results from these scans are recorded in Table 10 and focus on the minimal $\sum v_\infty$ compliant transit as the subjective criterion for an optimal λ_{31r}.

Table 10. The rightmost two columns apply to the 2LL -compliant transit with minimum $\sum v_\infty$ among *n* others tallied by each λ_{31r}-specific scan in the 2031 Earth/Mars opposition timeframe. The single-leg scan has no waypoint and is thus independent of λ_{31r}.

λ_{31r} (deg)	*n*	$\sum v_\infty$ (km/s)	Δt (days)
Single-leg	1143	7.226	235.0
-136.592	33	19.742	300.0
-126.592	24548	13.972	300.0
-116.592	37115	12.279	300.0
-106.592	3553	17.529	300.0
-96.592	0		

Each of the two-leg scans in Table 10 is associated with a minimum $\sum v_\infty$ transit whose RLP is the minimally compliant 5.0 days. All Table 10 two-leg scans also have Δt = 300.0 days because minimum $\sum v_\infty$ will generally be limited by the imposed Δt_{Max} value in this paper. Owing to its maximum *n* and minimum $\sum v_\infty$ among other two-leg scans in Table 10, λ_{31r} = -116.592° is selected as optimal for waypoint phasing in Mars-to-Earth transits beginning with the 2031 opposition's timeframe.

[6] This liberal limit's primary purpose is to quickly exclude "wrong way" retrograde heliocentric trajectories from 2LL mission compliance.

Synodic-Resonant Earth/Mars Waypoints

For each "viable" opposition in Table 2 (namely those four with nearly zero $\Delta\lambda$), a 2LL scan is made with its waypoint coasted as a USSB from λ_{31r} = -116.592° initial conditions. Each of these is supplemented by a single-leg scan with the same control values for comparison purposes. Furthermore, all 2LL control values are held at those previously given except for the six-month Leg-C departure interval from t_{Di} to t_{Df}. This interval slips to end near the Earth/Mars opposition epoch being assessed.

Results of the four 2LL scans, together with their single-leg counterparts, are summarized in Table 11 for transits with minimal $\sum v_\infty$ in the viable Leg-C departure intervals.

Table 11. The rightmost two columns apply to the 2LL -compliant transit with minimum $\sum v_\infty$ among n others tallied by each scan in the corresponding Earth/Mars opposition timeframe. Sums in the Δt column correspond to Leg-C + RLP + Leg-D durations. A single-leg scan has no waypoint and is thus independent of λ_{31r}.

t_{Di} to t_{Df} UTC Dates	2LL Scan Mode	n	$\sum v_\infty$ (km/s)	Δt (days)
1.0 Nov 2030 to 1.0 May 2031	Single-leg	1143	7.226	235
	λ_{31r} = -116.592°	37115	12.279	180 + 5 + 115 = 300
1.0 Mar 2035 to 1.0 Sep 2035	Single-leg	1359	5.980	195
	λ_{31r} = -116.592°	122296	8.774	145 + 5 + 150 = 300
1.0 Juy 2039 to 1.0 Jan 2040	Single-leg	972	5.950	285
	λ_{31r} = -116.592°	45527	12.224	170 + 5 + 125 = 300
1.0 Sep 2043 to 1.0 Mar 2044	Single-leg	913	7.122	300
	λ_{31r} = -116.592°	30051	12.857	185 + 5 + 110 = 300

The first Table 11 transit with minimum $\sum v_\infty$ whose waypoint is initialized at λ_{31} = -116.592° has its itinerary summarized in Table 12 and its heliocentric motion plotted in Figure 4. From the 2LL scan giving rise to this minimum $\sum v_\infty$ transit, the Figure 5 icicle plot is obtained.

Table 12. The following itinerary has a minimal $\sum v_\infty$ = 12.279 km/s among the n = 37115 2LL -compliant Leg-C/D transits departing Mars from 1.0 Nov 2030 to 1.0 May 2031 UTC. The associated waypoint is initialized at λ_{31r} = -116.592°. Phase Elapsed Time (PET) is reckoned from the Mars departure UTC date.

UTC Date	PET (d)	Event
01.0 Dec 2030	000.0	Leg-C Mars departure: v_∞ = 4.251 km/s
30.0 May 2031	180.0	Leg-C waypoint arrival: v_∞ = 3.364 km/s
04.0 Jun 2031	185.0	Leg-D waypoint departure: v_∞ = 2.195 km/s
27.0 Sep 2031	300.0	Leg-D Earth arrival: v_∞ = 2.469 km/s

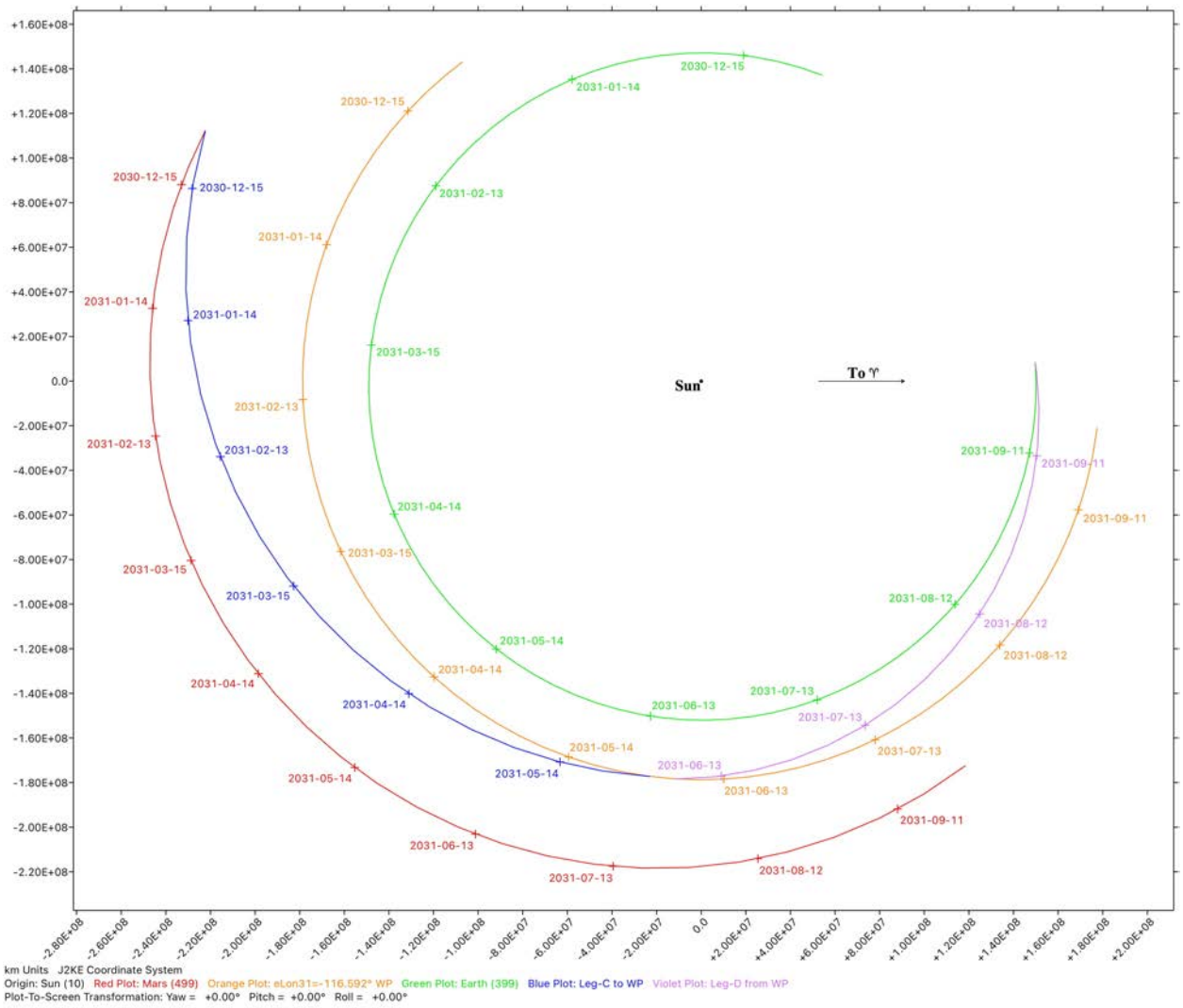

Figure 4. Inertial heliocentric ecliptic plane motion of the Earth (green), waypoint (orange), and Mars (red) is accompanied by Leg-C (blue) and Leg-D (purple) from the Table 12 transit itinerary. Time ticks ("+" markers) are annotated with 00:00 UTC dates in YYYY-MM-DD format at 30-day intervals. The direction annotated "To ♈" points along zero ecliptic longitude λ.

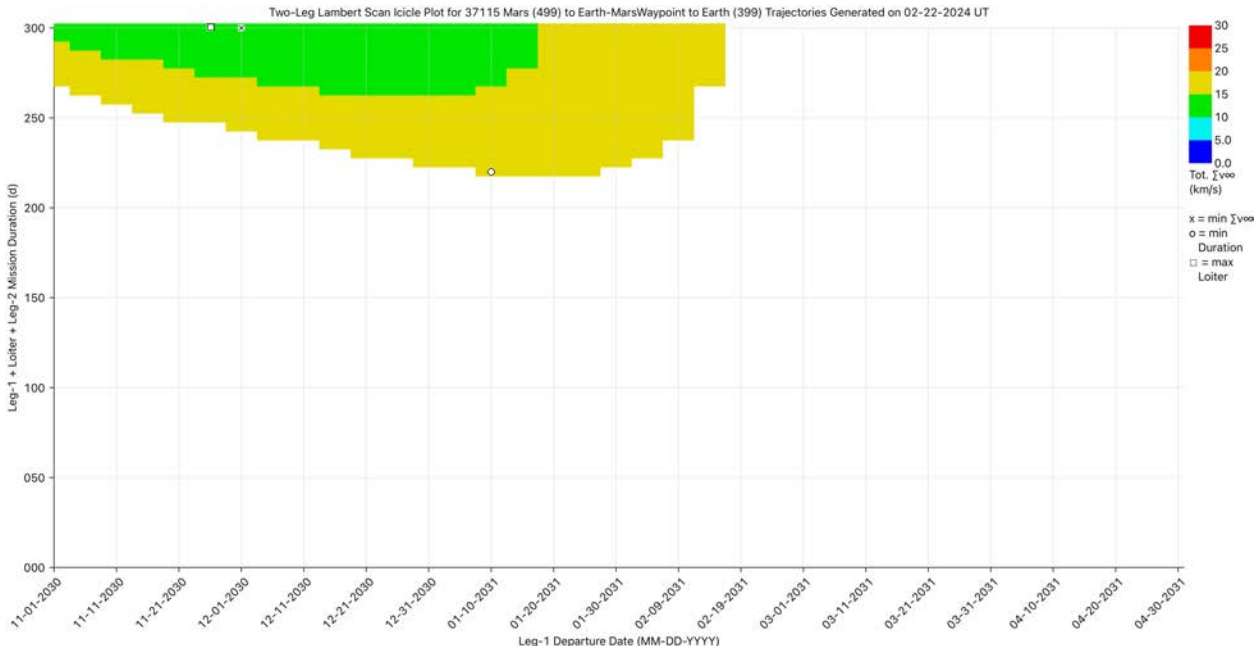

Figure 5. In this icicle plot, Leg C/D transit duration Δt is plotted against Mars departure date t_D and colored according to $\sum v_\infty$ as defined in the legend at upper right. The transit with minimum $\sum v_\infty$, detailed in Table 12 and Figure 4, is annotated by the black "x" marker at top left.

Return transits associated with Table 2 opposition periods beginning in 2031 having $\Delta\lambda$ near ±180° are serviced by a waypoint orbit initialized at λ_{31r} = -116.592°. Can a λ_{33r} waypoint orbit initialization be developed for interleaved oppositions beginning in 2033? To do so, retain all the 2LL control values adopted for λ_{31r} development except for the first two defining the Earth departure interval.

1) t_{Di} = 1.0 Jan 2033 UTC
2) t_{Df} = 1.0 Juy 2033 UTC

A single-leg 2LL scan is made with these control values as well. Results from λ_{33r} scans are recorded in Table 13 and focus on the minimal $\sum v_\infty$ compliant transit as the subjective criterion for an optimal λ_{33r}.

Table 13. The rightmost two columns apply to the 2LL -compliant transit with minimum $\sum v_\infty$ among *n* others tallied by each λ_{33r}-specific scan in the 2033 Earth/Mars opposition timeframe. The single-leg scan has no waypoint and is thus independent of λ_{33r}.

λ_{33r} (deg)	*n*	$\sum v_\infty$ (km/s)	Δt (days)
Single-leg	1360	6.033	215
-83.770	7696	16.576	300
-73.770	59851	11.398	300
-63.770	56635	11.310	300
-53.770	5653	17.258	300
-43.770	0		

Each of the two-leg scans in Table 13 is associated with a minimum $\sum v_\infty$ transit whose RLP is the minimally compliant 5.0 days. Owing to its nearly maximum n and minimum $\sum v_\infty$ among other two-leg scans in Table 13, λ_{33r} = -63.770° is selected as optimal for waypoint phasing in Mars-to-Earth transits beginning with the 2033 opposition's timeframe.

For each "viable" opposition in Table 2 (namely those four with nearly ±180° $\Delta\lambda$), a 2LL scan is made with its waypoint coasted as a USSB from λ_{33r} = -63.770° initial conditions. Each of these is supplemented by a single-leg scan with the same control values for comparison purposes. Furthermore, all 2LL control values are held at those previously given except for the six-month Leg-C departure interval ending at the approximate Earth/Mars opposition epoch being assessed.

Results of the four 2LL scans, together with their single-leg counterparts, are summarized in Table 14 for transits with minimal $\sum v_\infty$ in the viable Leg-C departure intervals. Table 14 two-leg transit results appear equally viable compared to intervening transits appearing in Table 11.

Table 14. The rightmost two columns apply to the 2LL -compliant transit with minimum $\sum v_\infty$ among n others tallied by each scan in the corresponding Earth/Mars opposition timeframe. Sums in the Δt column correspond to Leg-C + RLP + Leg-D durations. A single-leg scan has no waypoint and is thus independent of λ_{33r}.

t_{Di} to t_{Df} UTC Dates	2LL Scan Mode	n	$\sum v_\infty$ (km/s)	Δt (days)
1.0 Jan 2033 to 1.0 Juy 2033	Single-leg	1360	6.033	215
	λ_{33r} = -63.770°	56635	11.310	160 + 5 + 135 = 300
1.0 May 2037 to 1.0 Nov 2037	Single-leg	1144	6.930	270
	λ_{33r} = -63.770°	122832	8.945	145 + 5 + 150 = 300
1.0 Juy 2041 to 1.0 Jan 2042	Single-leg	923	5.654	300
	λ_{33r} = -63.770°	31325	13.264	180 + 5 + 115 = 300
1.0 Nov 2045 to 1.0 May 2046	Single-leg	1049	7.507	245
	λ_{33r} = -63.770°	29952	12.441	180 + 5 + 115 = 300

It should be no surprise that the difference λ_{33r} - λ_{31r} = -63.770 - (-116.592) = +52.822° is near +60°. Successive Earth/Mars oppositions advance in ecliptic longitude by an average of +60° as documented in Section 2.0.

7.0 Candidate Earth/Mars Waypoints Among Known NEOs

The USSBs serving as idealized waypoints in Sections 5.0 and 6.0 suggest searches in JPL's Small Bodies Database (SBDB) for catalogued NEOs with semi-major axis a near 1.195 AU per Equation 5 (1.145 < a < 1.245 AU), low eccentricity (e < 0.1), and low ecliptic inclination (i < 2°).[7] As of 5 February 2024, four SBDB members of the Amor NEO orbit group satisfy all these search criteria.

Table 15 identifies Amors compliant with these criteria, estimates their diameters, and indicates how well they match optimal outbound (λ_{31} or λ_{33}) and return (λ_{31r} or λ_{33r}) waypoint phasing.

[7] An SBDB search can be performed at https://ssd.jpl.nasa.gov/tools/sbdb_query.html (accessed 5 February 2024).

The table is appended with (225312) 1996 XB_{27}, the only SBDB Amor NEO whose diameter is likely to exceed 100 m which still satisfies the $1.145 < a < 1.245$ AU and $e < 0.1$ search criteria. Also appended is (138911) 2001 AE_2, the only SBDB Amor likely to exceed 100 m diameter which still satisfies $e < 0.1$ and $i < 2°$ search criteria.

Table 15. Members of the Amor NEO orbit group best matching idealized USSB waypoints developed by this paper are identified. Estimated diameter range *d* is computed based on absolute magnitude and an assumed albedo range from 0.3 (more reflective and therefore smaller) to 0.05 (less reflective and therefore larger).[8] For comparison purposes, values within the heading's {curly braces} apply to an ideal waypoint as developed in this paper.

Name	*d* (m)	*a* (AU) {1.195}	*e* {0}	*i* {0}	λ_{31}, λ_{31r} {-157°, -117°}	λ_{33}, λ_{33r} {-94°, -64°}
2009 OS_5	32 to 79	1.148	0.0994	1.71°	-162.3°	+112.3°
2014 KD_{45}	7 to 16	1.153	0.0923	0.77°	+118.9°	+37.6°
2020 MB	31 to 75	1.187	0.0538	1.68°	+64.2°	+64.2°
2021 EN_5	12 to 28	1.152	0.0852	0.28°	-113.9°	+148.9°
1996 XB_{27}	100 to 245	1.189	0.0581	2.47°	-89.1°	+138.2°
2001 AE_2	316 to 774	1.35	0.0817	1.66°	-119.3°	+14.1°

Despite its excessive *a*, how well might 2001 AE_2 serve as a return waypoint during Table 2 opposition timeframes with near-zero $\Delta\lambda$? Using 2LL control values from Section 6.0, the only 2LL scan of 2001 AE_2 with *n* not zero has results appearing in Table 16.[9]

Table 16. The rightmost two columns apply to the 2LL -compliant return transit with minimum $\sum v_\infty$ among *n* others tallied by scans in the 2031 Earth/Mars opposition timeframe. Sums in the Δt column correspond to Leg-C + RLP + Leg-D durations. The λ_{31r} = -119.334° scan pertains to a return transit via Amor NEO (138911) 2001 AE_2. A single-leg scan has no waypoint and is thus independent of λ_{31r}. No other compliant transits via 2001 AE_2 are found in scans during the 2035, 2040, or 2044 opposition timeframes.

t_{Di} to t_{Df} UTC Dates	2LL Scan Mode	*n*	$\sum v_\infty$ (km/s)	Δt (days)
1.0 Nov 2030 to 1.0 May 2031	Single-leg	1143	7.226	235
	λ_{31r} = -119.334°	12206	15.055	160 + 5 + 135 = 300

The paucity of 2LL-compliant return transits in Table 16 indicates *a* is critical to a waypoint's utility through regular reuse. To test this hypothesis, actual 2001 AE_2 heliocentric semi-major axis is changed to match the synodic-resonant value from Equation 5. This modification is performed at the 04.497 May 2031 UTC Earth/Mars opposition epoch from Table 2 to preserve heliocentric position and λ_{31r} = -119.334°.

[8] Reference https://cneos.jpl.nasa.gov/tools/ast_size_est.html (accessed 5 February 2024).
[9] Analysis and modification of the 2001 AE_2 orbit is based on the JPL#201 *Horizons* ephemeris.

Synodic-Resonant Earth/Mars Waypoints

A synodic-resonant USSB dubbed "res2001ae2" is produced by modification of 2001 AE_2's a. Its 2LL scan results, using control values from Section 6.0, appear in Table 17. Note the dramatic increase in n for all the Mars departure intervals with respect to Table 16, demonstrating the sensitivity of waypoint reuse to synodic resonance. Nevertheless, comparison of Table 17's two-leg minimum $\sum v_\infty$ values with corresponding values in Table 11 indicates res2001ae2 is less accessible than the idealized waypoint orbit initialized with λ_{31r} = -116.592°, zero eccentricity, and zero ecliptic inclination.

Table 17. The rightmost two columns apply to the 2LL-compliant transit through idealized resonant waypoint res2001ae2 with minimum $\sum v_\infty$ among n others tallied by each scan in the corresponding Earth/Mars opposition timeframe. Sums in the Δt column correspond to Leg-C + RLP + Leg-D durations. A single-leg scan has no waypoint and is thus independent of λ_{31r}.

t_{Di} to t_{Df} UTC Dates	2LL Scan Mode	n	$\sum v_\infty$ (km/s)	Δt (days)
1.0 Nov 2030 to 1.0 May 2031	Single-leg	1143	7.226	235
	λ_{31r} = -119.334°	14614	14.685	170 + 5 + 125 = 300
1.0 Feb 2035 to 1.0 Aug 2035	Single-leg	1359	5.980	195
	λ_{31r} = -119.334°	170141	10.052	165 + 5 + 130 = 300
1.0 Jun 2039 to 1.0 Dec 2039	Single-leg	972	5.950	285
	λ_{31r} = -119.334°	9148	16.622	190 + 5 + 105 = 300
1.0 Sep 2043 to 1.0 Mar 2044	Single-leg	913	7.122	300
	λ_{31r} = -119.334°	5067	16.376	180 + 5 + 115 = 300

By changing 2001 AE_2 a to achieve synodic resonance without any position change, the change in velocity magnitude Δv = 1.589 km/s between 2001 AE_2 and res2001ae2 is easily computed at 04.497 May 2031 UTC when their orbits intersect. This Δv is an impulsive approximation of the propulsion required to achieve synodic resonance for 2001 AE_2. Consider the following simulation of this impulse based on currently available SpaceX Raptor engine attributes.

$g \equiv$ Earth surface gravity acceleration = 0.0098067 km/s^2
$I_{SP} \equiv$ propulsive specific impulse = 363 s[10]
$v_{EX} \equiv$ propulsive exhaust speed = $g\ I_{SP}$ = 3.559832 km/s
$m_i \equiv$ estimated 2001 AE_2 mass = 7.329E+10 kg[11]

With Δv = 1.589 km/s imparted to 2001 AE_2 under these assumptions, and using propellant only from the asteroid, the rocket equation determines res2001ae2's post-impulse mass m_f as follows.

$$m_f = m_i e^{-\Delta v / v_{EX}} = 4.691\text{E+10 kg}$$

Thus, this simulation finds about 36% of 2001 AE_2's mass would be consumed as propellant in achieving the res2001ae2 orbit. Even should such usable propellant mass be available on this

[10] Reference https://en.wikipedia.org/wiki/SpaceX_Raptor (accessed 8 February 2024).
[11] Reference https://en.wikipedia.org/wiki/101955_Bennu (accessed 8 February 2024). Asteroid (101955) Bennu 1999 RQ_{36} has a mean diameter of 490 m, in the range estimated for 2001 AE_2.

asteroid, achieving the res2001ae2 orbit is a formidable task. It may be more practical to construct a less massive waypoint from scratch in one of the ideal orbits identified by Sections 5.0 and 6.0. This waypoint would initially use Earth-supplied infrastructure and subsequently obtain additional resources from Amors such as those in Table 15. As discussed in Section 11.0, new survey capabilities to become operational this decade will significantly increase NEO discovery rates. These discoveries will likely produce many more natural waypoint candidates and resources accessible to waypoints regardless of their respective pedigrees.

8.0 Rediscovered Virtues Of Staging In A Waypoint Context

Consider an interplanetary human transport based on currently available SpaceX Starship attributes.[12]

$g \equiv$ Earth surface gravity acceleration = 0.0098067 km/s^2
$I_{SP} \equiv$ propulsive specific impulse = 380 s
$v_{EX} \equiv$ propulsive exhaust speed = $g\ I_{SP}$ = 3.726546 km/s
$\Delta v \equiv$ change-in-velocity magnitude to be imparted by propulsion in km/s
$m_Y \equiv$ payload mass in kg
$m_i \equiv$ dry/inert mass = 100000 kg
$m_P \equiv$ propellant mass in kg
$m_X \equiv$ maximum permissible total mass ($m_Y + m_i + m_P$) = 1300000 kg

A value for m_Y is sought such that $m_Y + m_i + m_P = m_X$ at an interplanetary departure before any propellant is expended. The rocket equation provides the desired solution.

$$m_X = (m_Y + m_i)e^{\Delta v/v_{EX}} \longrightarrow m_Y = m_X e^{-\Delta v/v_{EX}} - m_i \tag{6}$$

Next, conduct single-leg and Table 6 Leg-A/B simulated transits based on minimum $\sum v_\infty$ solutions from corresponding outbound 2LL scans with Earth departures in the 2030-31 timeframe. These simulations adopt the following assumptions,[13] and inputs/results are summarized in Table 18.

1) Earth departure/arrival begins/ends in a circular parking orbit of radius r_E = 6563.137 km subject to gravitation from reduced mass μ_E = 398600.435436 km^3/s^2. Departure/arrival change-in-velocity magnitude is
$$\Delta v_E = \sqrt{\frac{2\mu_E}{r_E} + v_\infty^2} - \sqrt{\frac{\mu_E}{r_E}}, \tag{7}$$
where v_∞ applies to the pertinent single/two-leg Earth asymptotic speed.
2) Arrival and departure change-in-velocity magnitudes at the waypoint are defined to be the pertinent asymptotic speed because the waypoint has negligible mass.

[12] Reference https://en.wikipedia.org/wiki/SpaceX_Starship (accessed 25 January 2024). These attributes apply to the Starship spacecraft/second stage only.
[13] Note that Equations 7 and 8 will be used in multiple contexts, including arrivals/departures and single/two-leg transits. Consequently, subscripting in both equations is genericized to be agnostic of these contexts. When Equations 7 and 8 are referenced, the specific context will be made apparent.

3) Mars departure/arrival begins/ends in a circular parking orbit of radius r_M = 3778.1 km subject to gravitation from reduced mass μ_M = 42828.3752 km^3/s^2. Departure/arrival change-in-velocity magnitude is

$$\Delta v_M = \sqrt{\frac{2\mu_M}{r_M} + v_\infty^2} - \sqrt{\frac{\mu_M}{r_M}}, \quad (8)$$

where v_∞ applies to the pertinent single/two-leg Mars asymptotic speed.

Table 18. These two Earth-to-Mars simulations are based on minimal $\sum v_\infty$ transits obtained with 2LL scans in the 2031 opposition timeframe. Columns headed by m_{YAarr} and m_{YBarr} have maximum payload mass values in kg units produced by Equation 6. All other columns have values in km/s units.

Simulation	$v_{\infty Adep}$	Δv_E	$v_{\infty Aarr}$	m_{YAarr}	$v_{\infty Bdep}$	$v_{\infty Barr}$	Δv_M	m_{YBarr}
Single-leg	3.192	3.681				3.555	2.575	142566
Leg-A/B	2.331	3.472	1.775	218034	1.919	3.455	2.516	295439

The Table 18 single-leg simulation has a $\sum v_\infty$ = 6.747 km/s, while the Leg-A/B simulation has $\sum v_\infty$ = 9.480 km/s, a value 1.405 times greater as previously noted in association with Table 5 narrative. Nevertheless, the Table 18 payload mass deliverable to Mars (m_{YBarr}) by the Leg-A/B simulation is 2.072 times that deliverable with the single-leg simulation. Because at most a 218034 kg payload can be carried to the waypoint from Earth, a still more massive Mars payload delivery would likely entail a mixed payload manifest from Earth and the waypoint on Leg-B.

Both the single-leg simulation and Leg-B depart with total mass m_X = 1300000 kg. In accord with Table 18, the single-leg simulation imparts Δv = 3.681 + 2.575 = 6.256 km/s in reaching Mars from Earth. But the Leg-A/B simulation imparts Δv = 1.919 + 2.516 = 4.435 km/s in reaching Mars from the waypoint. Thus, more payload mass can be delivered to Mars with the Leg-A/B simulation, and this advantage with respect to the single-leg simulation is only magnified when I_{SP} < 380 s.

Table 18 is but another illustration of efficiencies realized through staging in off-Earth transport architecture. Someday, technology may advance to the point where a single-stage rocket can be launched from Earth to achieve a stable low-Earth orbit, but this feat has yet to be achieved. Although single-leg transport to Mars is possible with current technology, an intermediate waypoint capable of replenishing consumables permits significantly greater mass transport with a specified vehicle.

What of mass flow in the opposite Mars-to-Earth direction? Under the same assumptions as those supporting Table 18's simulations, single-leg and Table 12 Leg-C/D simulated transits based on minimum $\sum v_\infty$ solutions from corresponding return 2LL scans with Mars departures in the 2030-31 timeframe are assessed in Table 19.

Table 19. These two Mars-to-Earth simulations are based on minimal $\sum v_\infty$ transits obtained with 2LL scans in the 2031 opposition timeframe. Columns headed by m_{YCarr} and m_{YDarr} have maximum payload mass values in kg units produced by Equation 6. All other columns have values in km/s units.

Simulation	$v_{\infty Cdep}$	Δv_M	$v_{\infty Carr}$	m_{YCarr}	$v_{\infty Ddep}$	$v_{\infty Darr}$	Δv_E	m_{YDarr}
Single-leg	2.805	2.159				4.421	4.082	143558
Leg-C/D	4.251	3.016	3.364	134638	2.195	2.469	3.501	181906

As with the outward mass flow quantified in Table 18, a factor of 181906/143582 = 1.267 more mass can be delivered to Earth's vicinity by the Table 19 Leg-C/D simulation than its single-leg counterpart. Both the outbound Leg-A/B and inbound Leg-C/D simulations can take on additional payload mass during their waypoint loiter periods even if none of the arriving payload mass is offloaded.

In a sense, the Table 18/19 simulations are best cases because associated $\lambda_{31}/\lambda_{31r}$ values have been optimized to produce minimum $\sum v_\infty$ for transits in the same 2031 opposition timeframe (reference data in Tables 4/10) they reference. Such is also the case for optimized $\lambda_{33}/\lambda_{33r}$ values and transits circa 2033. How do two-leg transit deliverable payload masses compare with those from contemporaneous single-leg transits, both Earth-to-Mars and Mars-to-Earth, for all opposition timeframes in Table 1? Pertinent data appear in Tables 20 and 21.

Table 20. Phase elapsed time (PET) referenced to Earth departure, together with maximum deliverable payload mass m_Y, are listed for the minimum $\sum v_\infty$ single-leg and Leg-AB Earth-to-Mars transit in each Table 1 opposition spanning T_S. If a Leg-AB Mars arrival m_Y exceeds the contemporaneous single-leg value, it is colored green. Otherwise, it is colored red.

Opposition Year	Itinerary	Waypoint Arrival		Mars Arrival	
		PET (d)	m_Y (kg)	PET (d)	m_Y (kg)
2031	Single-leg			285	142566
	Leg-AB	145	218034	300	**295439**
2033	Single-leg			200	154848
	Leg-AB	145	198011	300	**351466**
2035	Single-leg			200	176938
	Leg-AB	120	195250	300	**63817**
2037	Single-leg			220	149804
	Leg-AB	125	194784	300	**155138**
2040	Single-leg			300	143770
	Leg-AB	120	179231	300	**69288**
2042	Single-leg			300	179238
	Leg-AB	115	101454	300	**84509**
2044	Single-leg			300	174951
	Leg-AB	125	176186	300	**153424**
2046	Single-leg			290	154442
	Leg-AB	130	118788	300	**109614**

Table 21. Phase elapsed time (PET) referenced to Mars departure, together with maximum deliverable payload mass m_Y, are listed for the minimum $\sum v_\infty$ nonstop and Leg-CD Mars-to-Earth transit in each Table 1 opposition spanning T_S. If a Leg-CD Earth arrival m_Y exceeds the contemporaneous nonstop value, it is colored green. Otherwise, it is colored red.

Opposition Year	Itinerary	Waypoint Arrival		Earth Arrival	
		PET (d)	m_Y (kg)	PET (d)	m_Y (kg)
2031	Single-leg			235	143558
	Leg-CD	180	134638	300	**181906**
2033	Single-leg			215	174623
	Leg- CD	160	157282	300	**211818**
2035	Single-leg			195	168506
	Leg- CD	145	281879	300	**217104**
2037	Single-leg			270	138276
	Leg- CD	145	286771	300	**174225**
2040	Single-leg			285	166496
	Leg- CD	170	146322	300	**113668**
2042	Single-leg			300	178882
	Leg- CD	180	96468	300	**112222**
2044	Single-leg			300	142240
	Leg- CD	185	108465	300	**140910**
2046	Single-leg			245	136992
	Leg- CD	180	119756	300	**175799**

If necessary, m_Y-deficient (**red**) cases in Tables 20/21 can at least partially be mitigated by increasing Δt_{Max} in associated 2LL scans. Furthermore, the process by which a waypoint's λ is optimized in Sections 5.0 and 6.0 is notional and easily modified. For example, the λ optimization figure of merit can be changed from a specific opposition timeframe's minimal $\sum v_\infty$ to the minimal sum of all four pertinent opposition timeframes' (2031, 2035, 2040, and 2044 for λ_{31} or λ_{31r}; 2033, 2037, 2042, and 2046 for λ_{33} or λ_{33r}) minimal $\sum v_\infty$ values. This optimization tends to reduce variations in maximum deliverable m_Y values for a waypoint.

Despite multiple m_Y-deficient cases in Tables 20/21, the overall trend in deliverable m_Y over a synodic sequence T_S clearly favors two-leg transfers over single-leg itineraries. Table 22 provides summations of m_Y values deliverable to waypoints and Mars from Table 20, and Table 23 provides summations of m_Y values deliverable to waypoints and Earth from Table 21.

Table 22. Summation of Table 20 Leg-AB Mars arrival m_Y values exceeds the contemporaneous single-leg Table 20 summation and is colored green.

Itinerary	Total m_Y Deliverable Over T_S (15 years)	
	To WP (kg)	To Mars (kg)
Single-leg		1276558
Leg-AB	1381738	**1282696**

Table 23. Summation of Table 21 Leg-CD Earth arrival m_Y values exceeds the contemporaneous single-leg Table 21 summation and is colored green.

Itinerary	Total m_Y Deliverable Over T_S (15 years)	
	To WP (kg)	To Earth (kg)
Single-leg		1249572
Leg-CD	1331582	**1327652**

With opportunities for additional supply and demand at waypoints between Earth and Mars, a two-leg interplanetary transport architecture can enable more than an increased flow of goods between the two planets. It also fosters completely new economic markets at waypoints where none would exist with direct Earth/Mars transport alone.

An analogous profitable flow of goods and services appears to be enabled by transcontinental air transport across the 48 contiguous United States. Per data presented in the Appendix, only 4% of bookable transcontinental itineraries (BTIs) on the four most patronized U.S. airlines are nonstop during the week beginning 2 June 2024. Despite longer transit times and increased fuel/ground processing costs, multi-stop BTIs must be more profitable than nonstop BTIs, or airlines favoring them so heavily would not remain in business for decades.

9.0 Waypoints As Earth/Mars Communications Relays

Current interplanetary communications technology requires a Sun-Mars-Earth elongation angle $\varepsilon' > 4°$ to ensure solar radiation does not interfere with radio signals [6, p. 2]. During the interval spanned by Table 1 entries, communication outage windows (COWs) open and close on UTC dates appearing in Table 24. As observed from Earth, Mars is in solar conjunction during each of these COWs.[14]

Table 24. Communications outage windows (COWs), during which the Sun-Mars-Earth elongation angle $\varepsilon' \leq 4°$ with the two planets on opposite sides of the Sun, open and close on the following UTC dates.

COW Open	COW Close	COW Duration (days)
20 Jun 2032	01 Aug 2032	42
30 Juy 2034	08 Sep 2034	40
04 Sep 2036	13 Oct 2036	39
12 Oct 2038	21 Nov 2038	40
25 Nov 2040	08 Jan 2041	44
26 Jan 2043	18 Mar 2043	51
07 Apr 2045	26 May 2045	49

Variations in Table 24 COW durations undergo a cycle resembling those of Table 1's ΔPET values. In both datasets, cyclic variations are due primarily to elevated eccentricity in the orbit of Mars.

[14] As observed from Mars, Earth is in *superior* conjunction with the Sun (on the opposite side of the Solar System) during each COW.

Synodic-Resonant Earth/Mars Waypoints

As illustrated by Figure 6, the two outbound and two return waypoints tend to be well removed from the Earth/Mars line during the first Table 24 COW. In this regard, any of the waypoints developed in Sections 5.0 and 6.0 can function as an effective communications relay between Earth and Mars during the 2032 COW. Five synodic periods later, similar effective relay geometry is illustrated by Figure 7 for the 2043 COW.

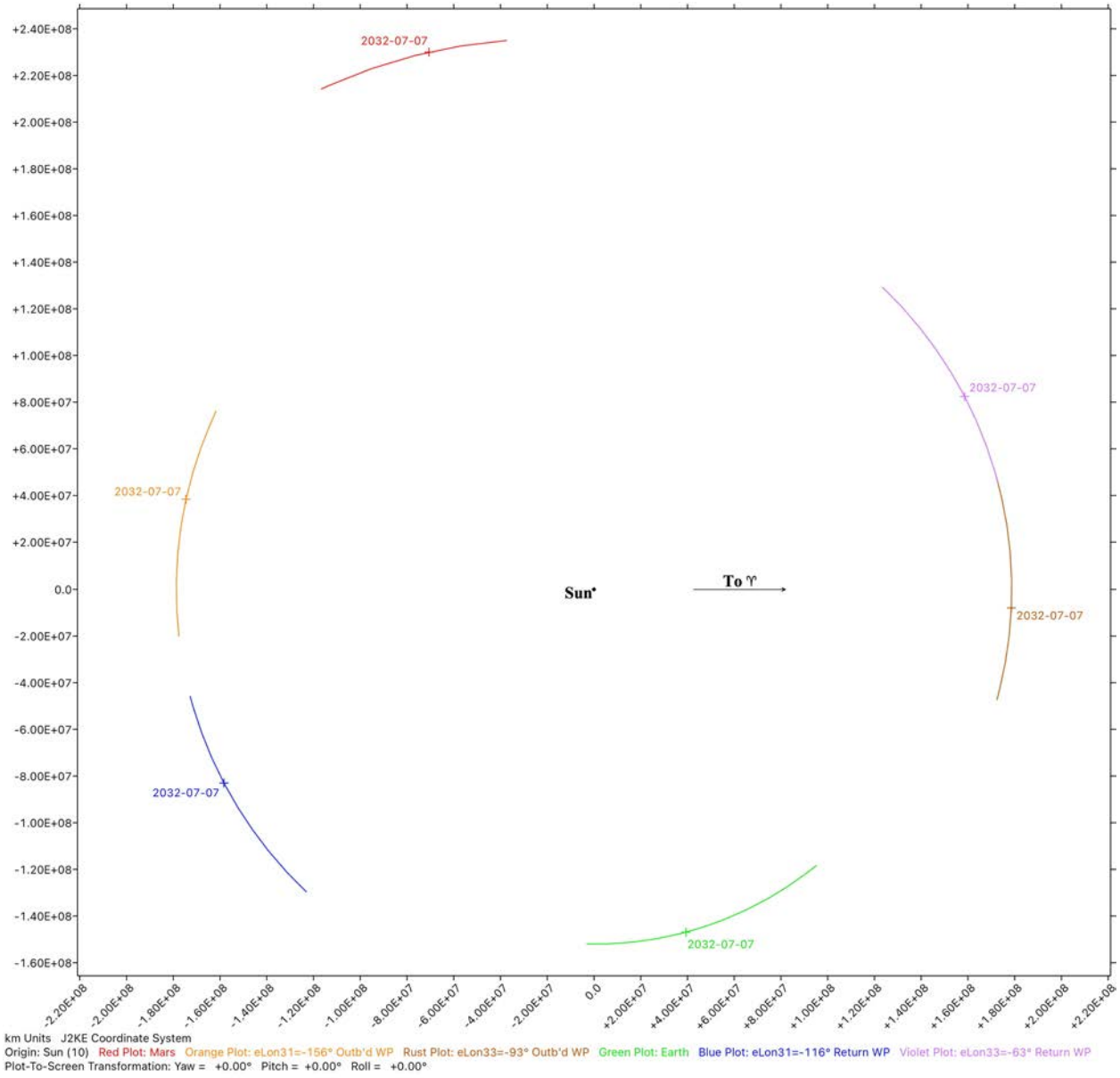

Figure 6. Inertial heliocentric ecliptic plane motion of the Earth (green), Mars (red), and four previously defined waypoints is plotted during the 42-day COW from 20 June to 1 August 2032. Outbound waypoints (reference Section 5.0) are colored orange and rust, while return waypoints (reference Section 6.0) are colored blue and violet. Time ticks ("+" markers) are annotated with a 00:00 UTC date in YYYY-MM-DD format. The direction annotated "To ♈" points along zero ecliptic longitude λ.

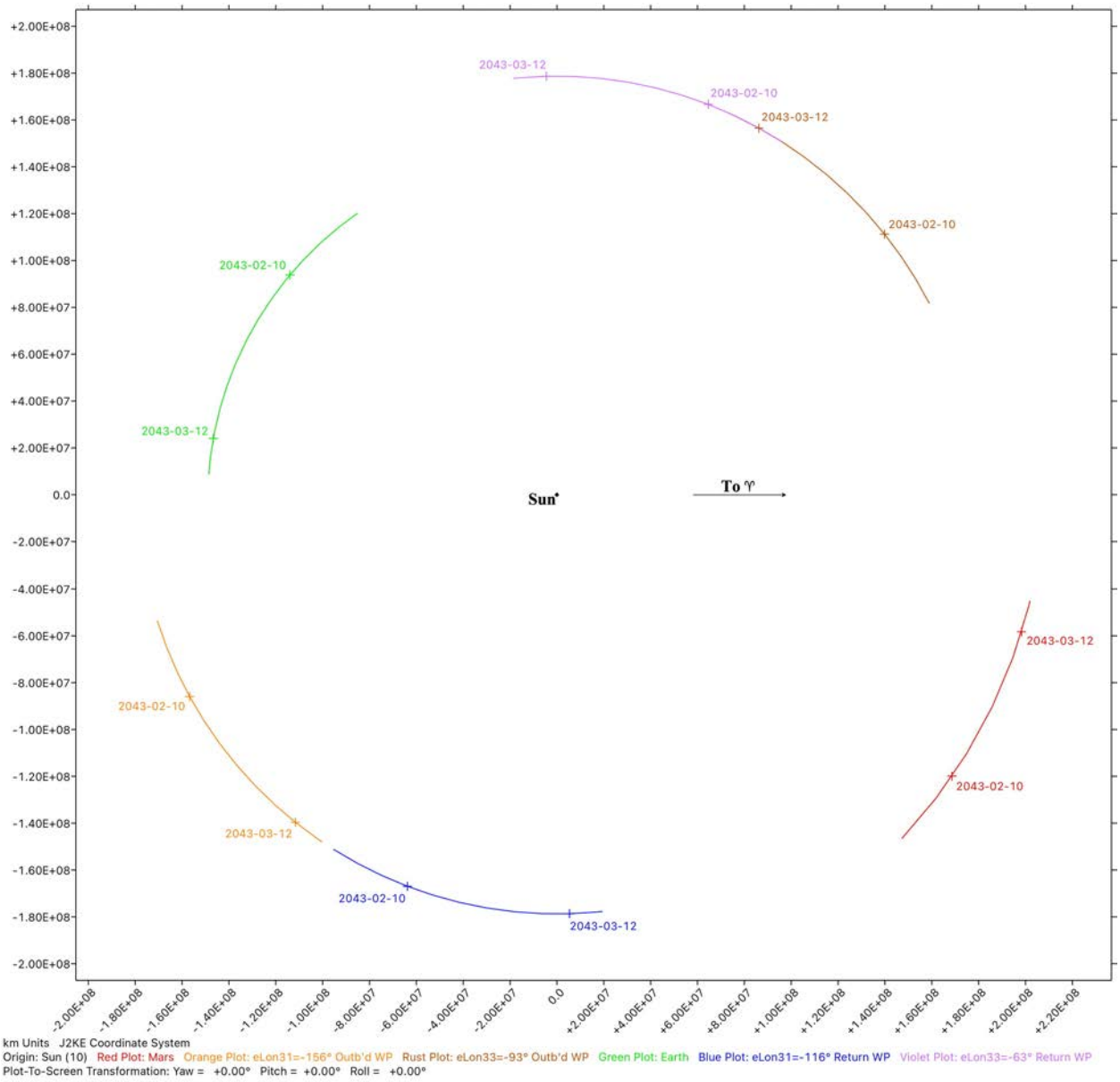

Figure 7. Inertial heliocentric ecliptic plane motion of the Earth (green), Mars (red), and four previously defined waypoints is plotted during the 51-day COW from 26 January to 18 March 2043. Outbound waypoints (reference Section 5.0) are colored orange and rust, while return waypoints (reference Section 6.0) are colored blue and violet. Time ticks ("+" markers) are annotated with 00:00 UTC dates in YYYY-MM-DD format at 30-day intervals. The direction annotated "To ♈" points along zero ecliptic longitude λ.

10.0 Interplanetary Aborts Facilitated By Waypoints

Either Leg-A/B or Leg-C/D of a two-leg transit reaches its targeted destination in less time than does a single-leg transit. As presented in Tables 5, 9, 11, and 14 for comparable minimum $\sum v_\infty$ transits, Δt data indicate Leg-A, B, C, and D durations never exceed 145, 180, 185, and 150 days,

respectively. Meanwhile, these data for single-leg transits are never less than 200 days outbound nor 195 days on return. Therefore, time-critical forward aborts to the nominal destination tend to be more robust in a two-leg transit than in a single-leg transit.

In contrast, ensuing subsections each focus on more subtle consequences from a turnaround abort scenario in which a mishap occurs in interplanetary space and return to the point of departure is sought. Given the scenario's planned/nominal trajectory, when is the time of latest turnaround (TLT) and how does this time differ between single-leg trajectories and their two-leg counterparts utilizing waypoints? Example aborts are initiated on nominal outbound/return trajectories following the Δv_{dep} impulse and adopt Raptor/Starship performance data as previously disclosed in Section 8.0. Any abort entails three events. First, m_Y as computed by Equation 6 is jettisoned. Subsequently, post-abort turnaround Δv_{AT} and abort arrival Δv_{AA} impulses are performed.

The condition for each abort's viability is an abort arrival mass m_{AA+} exceeding m_i = 100000 kg per Section 8.0. Abort impulses are computed from heliocentric Lambert solutions to form a two-dimensional grid with each column being the UTC at which Δv_{AT} is applied and each row being the UTC at which Δv_{AA} is applied. This grid is called a porkchop chart (PCC), and its column/row UTC intervals are fixed at 10 days. Two types of PCC datasets are produced covering distinct ranges of heliocentric transfer angles from Δv_{AT} to Δv_{AA}. First is the "partial-rev, short-way" dataset covering transfers greater than zero and less than 180°, while second is the "partial-rev, long-way" dataset covering transfers greater than 180° and less than 360°. If the abort targets an Earth arrival, the corresponding Lambert solution's v_∞ value is used with Equation 9 to compute Δv_{AA}.

$$\Delta v_{AA} = \sqrt{\frac{2\mu_E}{r_E} + v_\infty^2} - \sqrt{\frac{2\mu_E}{r_E}} \tag{9}$$

Abort arrival at Mars uses Equation 10 to compute Δv_{AA} with that v_∞.

$$\Delta v_{AA} = \sqrt{\frac{2\mu_M}{r_M} + v_\infty^2} - \sqrt{\frac{2\mu_M}{r_M}} \tag{10}$$

Equations 9 and 10 differ from their Equations 7 and 8 counterparts only in the second terms' additional $\sqrt{2}$ factor. With this factor, an abort arrival only seeks to achieve minimal gravitational capture at Earth or Mars.[15] In Leg-B or Leg-D abort arrivals at a waypoint, whose gravity field is effectively zero, Δv_{AA} is equivalent to the pertinent v_∞.

Since all aborts for a particular scenario have the nominal Δv_{dep} in common, their common mass at abort initiation (including payload jettison) is computed as follows.

[15] Consequently, abort examples in this section that are marginal with respect to the $m_{AA+} > m_i$ viability criterion will likely require in-space crew rescue upon arrival at Earth or Mars.

$$m_{AT-} = m_X e^{-\Delta v_{dep}/v_{EX}} - m_Y \quad (11)$$

Each specific abort case in the PCC can then compute its arrival mass with Equation 12.

$$m_{AA+} = m_{AT-} e^{-(\Delta v_{AT} + \Delta v_{AA})/v_{EX}} \quad (12)$$

In almost all scenarios without compromised propulsion, performing the Δv_{AT} impulse immediately after Δv_{dep} will initiate a viable abort. However, any Δv_{AT} less than 10 days after nominal departure is out of scope for the heliocentric Lambert solutions under study in this paper.[16]

10.1 Outbound Single-Leg Abort

The nominal trajectory for this scenario is consistent with Table 18's single-leg data. It departs Earth on 31.0 December 2030 UTC and arrives at Mars on 12.0 October 2031 UTC. With v_∞ set to $v_{\infty dep}$ = 3.192 km/s, Equation 7 provides Δv_E = 3.681 km/s. At nominal Mars arrival, v_∞ is set to $v_{\infty arr}$ = 3.555 km/s, and Equation 8 produces Δv_M = 2.575 km/s. In this case, Equation 6 sets m_Y = 142566 kg, and Equation 11 yields m_{AT-} = 341563 kg.

The PCC with partial-rev, short-way Lambert solutions and Equation 12 m_{AA+} values for this abort scenario is reproduced in Figure 8, where TLT is 1 March 2031 or 60 days after nominal Earth departure. Corresponding partial-rev, long-way Lambert solutions can delay TLT to 90 days after departure, but these late aborts are considered less practical because Earth arrival must be delayed until early 2032. Particularly in time-critical scenarios, a more advisable abort strategy might well be to remain on the nominal trajectory and arrive at Mars months earlier.

[16] Aborts performed so soon after departure may only briefly enter interplanetary space if they do so at all.

	A	B	C	D	E	F	G	H
1	**Abort Arrive**	**Abort Turnaround Date**						
2	**Date**	10-Jan-2031	20-Jan-2031	30-Jan-2031	9-Feb-2031	19-Feb-2031	1-Mar-2031	11-Mar-2031
3	20-Jan-2031	55013.9						
4	30-Jan-2031	93357.0	17841.4					
5	9-Feb-2031	110395.2	58926.4	5484.3				
6	19-Feb-2031	120292.9	84821.4	37400.8	1780.0			
7	1-Mar-2031	127172.8	101918.4	66668.2	24648.9	658.5		
8	11-Mar-2031	132263.8	114122.5	88236.8	53712.0	16905.9	273.0	
9	21-Mar-2031	136433.3	123613.3	104596.6	77851.7	44082.3	11892.7	119.2
10	31-Mar-2031	140035.0	131497.0	117698.6	97080.2	69010.0	36014.5	8196.7
11	10-Apr-2031	143129.3	138089.3	128278.3	112165.2	88842.6	59231.2	27786.2
12	20-Apr-2031	146033.5	143944.7	137213.6	124281.9	104212.5	77666.9	47465.3
13	30-Apr-2031	148800.8	149291.4	144955.4	134152.1	115995.5	91336.8	62790.7
14	10-May-2031	151464.5	154164.1	151586.1	142012.3	124701.7	100907.8	73483.2
15	20-May-2031	154316.3	158928.9	157553.1	148465.6	131213.4	107586.1	80769.7
16	30-May-2031	157467.6	163679.2	162956.8	153721.1	135970.1	112093.3	85562.4
17	9-Jun-2031	161207.3	168439.1	167689.8	157739.7	139167.3	114916.4	88598.7
18	19-Jun-2031	166209.1	173260.6	171678.3	160589.1	141109.8	116566.0	90532.3
19	29-Jun-2031	171475.4	176290.8	173604.1	161594.2	141603.8	117119.5	91574.2
20	9-Jul-2031	84326.2	163097.3	168337.8	158704.5	139898.4	116406.4	91837.3
21	19-Jul-2031	0.0	42246.8	135654.4	146211.1	134209.7	113884.1	91206.1
22	29-Jul-2031	0.0	0.0	28829.3	107562.3	119628.3	107973.9	89136.3
23	8-Aug-2031	0.0	0.0	0.0	22324.9	84132.9	94805.6	84396.4

Figure 8. This PCC provides m_{AA+} arrival mass values in kg for partial-rev, short-way turnaround abort cases from a nominal Earth-to-Mars single-leg transit. Cells with $m_{AA+} > m_i = 100000$ kg are colored green in this PCC, while cells failing to meet this criterion are colored red and correspond to inviable abort cases. The boxed Cell C19 has maximum m_{AA+} in the PCC. Aborts from this dataset can be initiated as late as 1 March 2031, 60 days after nominal Earth departure.[17]

10.2 Leg-A Abort

The nominal trajectory for this scenario is consistent with Table 18's Leg-A data. It departs Earth on 16.0 December 2030 UTC and arrives at the $\lambda_{31} = -156.592°$ waypoint on 10.0 May 2031 UTC. With v_∞ set to $v_{\infty dep} = 2.331$ km/s, Equation 7 provides $\Delta v_E = 3.472$ km/s. At nominal waypoint arrival, $v_{\infty arr} = \Delta v_{arr} = 1.775$ km/s. In this case, Equation 6 sets $m_Y = 218034$ kg, and Equation 11 yields $m_{AT-} = 294040$ kg.

The PCC with partial-rev, short-way Lambert solutions and Equation 12 m_{AA+} values for this abort scenario is reproduced in Figure 9, where TLT is 15 January 2031 or 30 days after nominal Earth departure. Abort arrival dates after the nominal transit's waypoint arrival in early May 2031 could be hard to justify, particularly in time-critical scenarios.

Why does the TLT for this Leg-A transit arise 30 days sooner with respect to Earth departure than does the single-leg scenario in Subsection 10.1? After all, Leg-A nominally has $\Delta v = \Delta v_{dep} + \Delta v_{arr} = 5.247$ km/s, while the single-leg transit's Δv is nominally 6.256 km/s.

[17] Empty cells in this and subsequent PCCs correspond to aborts whose arrive dates are on or before their turnaround dates. Many m_{AA+} values are effectively zero for later arrive dates because these short-way abort trajectories have retrograde heliocentric motion with respect to that of the Earth, Mars, and waypoints.

	A	B	C	D	E
1	**Abort Arrive**	**Abort Turnaround Date**			
2	**Date**	26-Dec-2030	5-Jan-2031	15-Jan-2031	25-Jan-2031
3	5-Jan-2031	75934.5			
4	15-Jan-2031	108190.4	29646.4		
5	25-Jan-2031	120027.8	67991.7	8842.3	
6	4-Feb-2031	125446.9	85609.8	37654.4	1866.3
7	14-Feb-2031	128454.7	94738.5	56286.6	17934.3
8	24-Feb-2031	130233.0	99994.9	67153.9	33673.0
9	6-Mar-2031	131352.9	103242.9	73768.9	44297.2
10	16-Mar-2031	132244.7	105619.8	78344.7	51597.6
11	26-Mar-2031	132926.4	107441.0	81732.4	56873.0
12	5-Apr-2031	133552.7	108994.2	84465.4	60950.3
13	15-Apr-2031	134195.8	110499.2	86977.8	64517.3
14	25-Apr-2031	134777.6	111882.9	89251.9	67671.9
15	5-May-2031	135413.1	113285.6	91467.5	70650.9
16	15-May-2031	136076.8	114739.1	93729.6	73644.1
17	25-May-2031	136708.2	116138.4	95903.4	76511.5
18	4-Jun-2031	137416.1	117614.9	98140.1	79419.8
19	14-Jun-2031	138134.5	119135.5	100444.3	82414.1
20	24-Jun-2031	138837.8	120623.9	102694.7	85339.0
21	4-Jul-2031	0.0	122215.8	105053.8	88374.7
22	14-Jul-2031	0.0	0.0	107477.7	91501.9
23	24-Jul-2031	0.0	0.0	0.0	94598.1

Figure 9. This PCC provides m_{AA+} arrival mass values in kg for partial-rev, short-way turnaround abort cases from a nominal Leg-A transit. Cells with $m_{AA+} > m_i = 100000$ kg are colored green in this PCC, while cells failing to meet this criterion are colored red and correspond to inviable abort cases. The boxed Cell B20 has maximum m_{AA+} in the PCC. Aborts from this dataset can be initiated as late as 15 January 2031, 30 days after nominal Earth departure.

The primary cause of this apparent contradiction lies with m_Y's determination using Equation 6. This computation's implicit assumption is payload and propellant masses can be interchanged without restriction on a Starship, provided their sum is $m_X - m_i = 1200000$ kg at a nominal transit departure. When an abort is declared and m_Y is jettisoned, transits with larger payload mass allocations have less propellant mass available for Δv_{AT} and Δv_{AA} execution. Post-jettison m_{AT-} for Figure 9 aborts is 47523 kg less than that for Figure 8 aborts, and this mass difference is implicitly all usable abort propellant.

Furthermore, Δv_{AT} tends to be greater in a Leg-A abort than in an outbound single-leg abort. For example, the boxed abort case in Figure 9 has $\Delta v_{AT} = 2.794$ km/s, while that for Figure 8's boxed case is 2.356 km/s. Since Δv_{AT} tends to be much greater than Δv_{AA} for viable aborts in both datasets, Figure 8/9 boxed case Δv_{AT} values are minimal for those datasets as well. This Δv_{AT} bias favoring Figure 8 aborts over Figure 9 aborts is thought to result from Leg-A transits tending to have greater heliocentric speeds than their single-leg counterparts. The speed bias arises because an abort turnaround from Leg-A tends to be performed closer to the Sun than does a contemporaneous outbound single-leg abort turnaround.

10.3 Leg-B Abort

The nominal trajectory for this scenario is consistent with Table 18's Leg-B data. It departs the λ_{31} = -156.592° waypoint on 15.0 May 2031 UTC and arrives at Mars on 12.0 October 2031 UTC. With negligible gravity at the waypoint, $v_{\infty dep} = \Delta v_{dep}$ = 1.919 km/s. At nominal Mars arrival, v_∞ is set to $v_{\infty arr}$ = 3.455 km/s and Equation 8 provides Δv_M = 2.516 km/s. In this case, Equation 6 sets m_Y = 295439 kg, and Equation 11 yields m_{AT-} = 481347 kg.

The PCC with partial-rev, short-way Lambert solutions and Equation 12 m_{AA+} values for this abort scenario is reproduced in Figure 10, where TLT is 14 July 2031 or 60 days after nominal waypoint departure. Abort arrival dates after the nominal transit's Mars arrival in early October 2031 could be hard to justify, particularly in time-critical scenarios.

	A	B	C	D	E	F	G	H
1	**Abort Arrive**	**Abort Turnaround Date**						
2	**Date**	25-May-2031	4-Jun-2031	14-Jun-2031	24-Jun-2031	4-Jul-2031	14-Jul-2031	24-Jul-2031
3	4-Jun-2031	102384.6						
4	14-Jun-2031	171265.6	35798.4					
5	24-Jun-2031	203170.8	100535.1	11985.6				
6	4-Jul-2031	221150.9	141540.5	57296.8	3712.4			
7	14-Jul-2031	232550.8	167632.0	96112.5	31107.7	1022.7		
8	24-Jul-2031	240323.8	185221.0	124037.6	62757.9	15765.3	240.8	
9	3-Aug-2031	245873.8	197628.0	144083.1	88641.5	38867.6	7315.5	46.8
10	13-Aug-2031	249950.4	206650.6	158729.9	108504.9	60554.7	22550.5	3057.6
11	23-Aug-2031	252990.1	213330.6	169593.4	123587.2	78466.8	39197.0	12135.6
12	2-Sep-2031	255265.7	218313.5	177717.9	135034.4	92674.8	54133.0	23881.6
13	12-Sep-2031	256960.3	222027.6	183806.2	143721.8	103768.2	66599.4	35464.2
14	22-Sep-2031	258204.7	224776.6	188359.9	150309.4	112368.5	76682.7	45727.3
15	2-Oct-2031	259095.8	226787.0	191754.6	155308.2	119026.3	84729.6	54394.8
16	12-Oct-2031	259705.0	228229.2	194278.2	159119.3	124208.4	91143.0	61568.9
17	22-Oct-2031	260080.3	229225.8	196145.6	162052.8	128295.4	96303.7	67494.1
18	1-Nov-2031	260243.0	229850.8	197503.3	164334.5	131581.2	100534.8	72443.7
19	11-Nov-2031	260181.7	230125.3	198430.0	166110.0	134274.8	104087.2	76663.8
20	21-Nov-2031	259836.3	230004.4	198931.2	167447.2	136504.4	107136.0	80348.6
21	1-Dec-2031	259058.8	229344.2	198921.6	168331.0	138319.9	109784.0	83633.0
22	11-Dec-2031	257507.5	227819.2	198177.5	168641.5	139687.9	112062.7	86592.5
23	21-Dec-2031	254300.1	224695.3	196215.9	168095.1	140465.5	113924.8	89241.8
24	31-Dec-2031	246448.4	218096.0	191971.0	166097.4	140333.8	115216.0	91524.8
25	10-Jan-2032	215046.8	201811.2	182785.2	161360.2	138636.7	115605.0	93285.6
26	20-Jan-2032	0.0	142479.6	160370.0	150755.3	133966.4	114413.7	94195.9
27	30-Jan-2032	0.0	0.0	89969.0	125182.7	122980.5	110191.8	93583.9
28	9-Feb-2032	0.0	0.0	0.0	55392.7	96589.9	99547.6	90007.0

Figure 10. This PCC provides m_{AA+} arrival mass values in kg for partial-rev, short-way turnaround abort cases from a nominal Leg-B transit. Cells with $m_{AA+} > m_i$ = 100000 kg are colored green in this PCC, while cells failing to meet this criterion are colored red and correspond to inviable abort cases. The boxed Cell B18 has maximum m_{AA+} in the PCC. Aborts from this dataset can be initiated as late as 14 July 2031, 60 days after nominal waypoint departure.

10.4 Return Single-Leg Abort

The nominal trajectory for this scenario is consistent with Table 19's single-leg data. It departs Mars on 6.0 December 2030 UTC and arrives at Earth on 29.0 July 2031 UTC. With v_∞ set to $v_{\infty dep}$ = 2.805 km/s, Equation 8 provides Δv_M = 2.159 km/s. At nominal Earth arrival, v_∞ is set to $v_{\infty arr}$ = 4.420 km/s, and Equation 7 produces Δv_E = 4.081 km/s. In this case, Equation 6 produces m_Y = 143582 kg, and Equation 11 yields m_{AT-} = 584675 kg.

The PCC with partial-rev, short-way Lambert solutions and Equation 12 m_{AA+} values for this abort scenario is reproduced in Figure 11, where TLT is 6 March 2031 or 90 days after nominal Earth departure. Abort arrival dates after the nominal transit's Earth arrival in late July 2031 could be hard to justify, particularly in time-critical scenarios.

	A	B	C	D	E	F	G	H	I	J	K
1	**Abort Arrive**					**Abort Turnaround Date**					
2	**Date**	16-Dec-2030	26-Dec-2030	5-Jan-2031	15-Jan-2031	25-Jan-2031	4-Feb-2031	14-Feb-2031	24-Feb-2031	6-Mar-2031	16-Mar-2031
3	26-Dec-2030	105610.2									
4	5-Jan-2031	178890.2	30309.9								
5	15-Jan-2031	208843.8	105171.2	7570.4							
6	25-Jan-2031	224589.5	150713.3	57160.4	1747.7						
7	4-Feb-2031	234177.3	177639.1	103840.2	29205.9	377.2					
8	14-Feb-2031	240563.9	194842.0	136194.1	68494.1	14124.9	75.3				
9	24-Feb-2031	245077.4	206564.9	158360.6	101097.0	43258.2	6451.6	13.6			
10	6-Mar-2031	248401.6	214941.0	173999.2	125433.9	72475.3	26071.2	2757.8	2.2		
11	16-Mar-2031	250924.8	221137.8	185376.2	143390.4	96502.1	49962.8	14893.4	1087.6	0.3	
12	26-Mar-2031	252884.5	225843.7	193869.1	156778.6	115199.2	71786.1	32915.5	7986.0	388.7	0.0
13	5-Apr-2031	254434.8	229491.1	200342.3	166908.6	129573.8	89828.7	51332.0	20556.5	3970.9	123.3
14	15-Apr-2031	255680.5	232365.5	205360.9	174683.8	140648.0	104215.9	67619.9	35034.6	12053.5	1805.7
15	25-Apr-2031	256695.5	234663.5	209308.9	180730.5	149238.6	115554.1	81169.6	48827.8	22636.1	6564.6
16	5-May-2031	257534.0	236525.9	212456.0	185490.5	155960.6	124477.9	92146.7	60871.8	33577.9	13720.0
17	15-May-2031	258236.7	238055.8	214997.6	189283.2	161271.8	131528.3	100949.2	70954.5	43671.6	21816.2
18	25-May-2031	258834.7	239331.3	217078.8	192344.0	165514.4	137137.8	107997.6	79229.8	52452.4	29761.6
19	4-Jun-2031	259352.8	240412.5	218809.4	194849.4	168946.2	141644.5	113664.4	85972.1	59864.0	36986.9
20	14-Jun-2031	259811.0	241346.7	220274.6	196934.2	171763.7	145310.8	118259.0	91470.0	66034.8	43291.3
21	24-Jun-2031	260225.7	242172.0	221540.9	198702.7	174117.9	148340.0	122030.6	95984.1	71157.6	48679.2
22	4-Jul-2031	260611.1	242919.5	222661.3	200236.5	176125.9	150890.3	125177.1	99735.4	75432.0	53251.3
23	14-Jul-2031	260979.8	243615.3	223678.8	201599.7	177878.8	153084.3	127854.2	102904.9	79039.5	57142.2
24	24-Jul-2031	261343.2	244282.1	224628.8	202843.6	179447.9	155017.4	130183.4	105637.3	82134.9	60487.8
25	3-Aug-2031	261713.1	244940.5	225540.8	204009.1	180888.5	156763.3	132258.9	108046.7	84845.3	63411.3
26	13-Aug-2031	262101.7	245609.8	226440.4	205129.1	182243.7	158377.9	134152.6	110221.4	87271.9	66017.2
27	23-Aug-2031	262523.4	246309.8	227349.9	206229.7	183545.7	159902.7	135917.9	112228.1	89493.5	68390.3
28	2-Sep-2031	262996.4	247061.8	228289.7	207330.6	184816.7	161365.9	137591.8	114114.6	91568.5	70596.7
29	12-Sep-2031	263545.4	247890.6	229277.9	208444.8	186068.3	162782.2	139195.7	115911.5	93537.3	72684.9
30	22-Sep-2031	264208.0	248826.8	230328.9	209574.3	187297.5	164149.7	140733.8	117631.9	95423.2	74687.1
31	2-Oct-2031	265043.9	249907.3	231446.8	210701.1	188477.1	165442.3	142187.5	119268.2	97230.4	76618.7
32	12-Oct-2031	266157.7	251170.9	232603.5	211760.5	189532.0	166591.2	143502.6	120783.7	98939.6	78475.9
33	22-Oct-2031	267742.3	252615.9	233660.9	212565.4	190279.0	167441.3	144559.8	122094.2	100497.3	80229.8
34	1-Nov-2031	270122.2	253918.5	234057.5	212560.6	190258.1	167643.0	145107.9	123027.8	101792.0	81813.5
35	11-Nov-2031	271942.6	251991.9	231175.1	209866.8	188193.1	166351.6	144597.6	123233.5	102604.9	83095.3
36											

Figure 11. This PCC provides m_{AA+} arrival mass values in kg for partial-rev, short-way turnaround abort cases from a nominal Mars-to-Earth single-leg transit. Cells with $m_{AA+} > m_i$ = 100000 kg are colored green in this PCC, while cells failing to meet this criterion are colored red and correspond to inviable abort cases. The boxed Cell B35 has maximum m_{AA+} in the PCC. Aborts from this dataset can be initiated as late as 6 March 2031, 90 days after nominal Mars departure.

10.5 Leg-C Abort

The nominal trajectory for this scenario is consistent with Table 19's Leg-C data. It departs Mars on 1.0 December 2030 UTC and arrives at the λ_{31} = -116.592° waypoint on 30.0 May 2031 UTC. With v_∞ set to $v_{\infty dep}$ = 4.251 km/s, Equation 8 provides Δv_M = 3.016 km/s. At nominal waypoint arrival, $v_{\infty arr} = \Delta v_{arr}$ = 3.364 km/s. In this case, Equation 6 sets m_Y = 134638 kg, and Equation 11 yields m_{AT-} = 444046 kg.

The PCC with partial-rev, short-way Lambert solutions and Equation 12 m_{AA+} values for this abort scenario is reproduced in Figure 12, where TLT is 31 December 2030 or 30 days after nominal Mars departure. Abort arrival dates after the nominal transit's waypoint arrival in late May 2031 could be hard to justify, particularly in time-critical scenarios.

	A	B	C	D	E
1	**Abort Arrive**	**Abort Turnaround Date**			
2	**Date**	11-Dec-2030	21-Dec-2030	31-Dec-2030	10-Jan-2031
3	21-Dec-2030	28934.4			
4	31-Dec-2030	69876.6	3542.5		
5	10-Jan-2031	89918.9	27663.3	350.5	
6	20-Jan-2031	100836.0	50592.5	9386.1	29.6
7	30-Jan-2031	107483.3	66377.0	25619.6	2825.3
8	9-Feb-2031	111852.6	77049.8	40522.1	11810.7
9	19-Feb-2031	114883.4	84467.1	52161.0	22979.2
10	1-Mar-2031	117072.0	89787.7	60931.2	33281.9
11	11-Mar-2031	118704.2	93716.7	67543.7	41855.5
12	21-Mar-2031	119956.1	96695.4	72591.9	48743.3
13	31-Mar-2031	120941.8	99010.2	76511.7	54233.6
14	10-Apr-2031	121738.3	100853.6	79614.6	58631.5
15	20-Apr-2031	122399.2	102358.3	82122.9	62196.2
16	30-Apr-2031	122962.8	103618.7	84197.2	65133.1
17	10-May-2031	123456.8	104702.7	85954.6	67600.7
18	20-May-2031	123901.8	105660.3	87481.6	69720.1
19	30-May-2031	124313.0	106528.6	88842.6	71583.8
20	9-Jun-2031	124701.9	107335.2	90086.1	73262.2
21	19-Jun-2031	125077.3	108101.1	91248.6	74809.4
22	29-Jun-2031	125445.5	108842.0	92357.8	76266.7
23	9-Jul-2031	125811.5	109569.9	93434.9	77665.8
24	19-Jul-2031	126179.2	110293.7	94495.7	79031.0
25	29-Jul-2031	126551.1	111020.3	95552.5	80380.8
26	8-Aug-2031	126929.6	111754.9	96614.3	81729.5
27	18-Aug-2031	127316.3	112501.2	97688.1	83087.8
28	28-Aug-2031	127712.5	113262.3	98779.0	84463.7
29	7-Sep-2031	128119.4	114040.2	99890.5	85862.8
30	17-Sep-2031	128538.4	114836.7	101025.3	87289.2
31	27-Sep-2031	128971.1	115653.0	102184.2	88744.7
32	7-Oct-2031	129419.8	116489.2	103366.4	90228.7
33	17-Oct-2031	129887.8	117342.4	104566.0	91735.4
34	27-Oct-2031	130376.6	118196.0	105762.4	93247.2
35	6-Nov-2031	130823.3	118949.0	106874.5	94707.9
36					

Figure 12. This PCC provides m_{AA+} arrival mass values in kg for partial-rev, short-way turnaround abort cases from a nominal Leg-C transit. Cells with $m_{AA+} > m_i$ = 100000 kg are colored green in this PCC, while cells failing to meet this criterion are colored red and correspond to inviable abort cases. The boxed Cell B35 has maximum m_{AA+} in the PCC. Aborts from this dataset can be initiated as late as 31 December 2030, 30 days after nominal Mars departure.

10.6 Leg-D Abort

The nominal trajectory for this scenario is consistent with Table 19's Leg-D data. It departs the λ_{31} = -116.592° waypoint on 4.0 June 2031 UTC and arrives at Earth on 27.0 September 2031 UTC. At nominal waypoint departure, $v_{\infty dep} = \Delta v_{dep}$ = 2.195 km/s. With v_∞ set to $v_{\infty arr}$ = 2.469 km/s, Equation 7 provides Δv_E = 3.501 km/s. In this case, Equation 6 sets m_Y = 181906 kg, and Equation 11 yields m_{AT-} = 539428 kg.

The PCC with partial-rev, short-way Lambert solutions and Equation 12 m_{AA+} values for this abort scenario is reproduced in Figure 13, where TLT is 3 August 2031 or 60 days after nominal waypoint departure. Abort arrival dates after the nominal transit's waypoint arrival in late September 2031 could be hard to justify, particularly in time-critical scenarios.

	A	B	C	D	E	F	G	H
1	**Abort Arrive**				**Abort Turnaround Date**			
2	**Date**	14-Jun-2031	24-Jun-2031	4-Jul-2031	14-Jul-2031	24-Jul-2031	3-Aug-2031	13-Aug-2031
3	24-Jun-2031	91202.2						
4	4-Jul-2031	164301.2	26659.2					
5	14-Jul-2031	199624.9	87452.1	7125.9				
6	24-Jul-2031	219776.2	129435.0	43900.6	1638.7			
7	3-Aug-2031	232587.9	156983.6	79912.7	20110.7	302.9		
8	13-Aug-2031	241314.5	175793.5	107227.1	45896.0	8119.2	42.1	
9	23-Aug-2031	247532.8	189129.6	127322.8	68761.7	23948.5	2795.4	4.1
10	2-Sep-2031	252092.4	198838.3	142178.3	87019.9	40662.7	11113.1	798.3
11	12-Sep-2031	255485.2	206009.4	153235.9	101161.2	55317.9	21831.4	4508.0
12	22-Sep-2031	258012.0	211317.8	161474.4	111973.7	67315.1	32319.1	10516.6
13	2-Oct-2031	259868.5	215210.1	167575.0	120162.5	76826.0	41508.8	17209.7
14	12-Oct-2031	261195.0	218012.0	172047.6	126317.7	84241.3	49156.4	23583.8
15	22-Oct-2031	262106.1	219988.6	175305.6	130940.8	89997.1	55377.8	29226.6
16	1-Nov-2031	262706.2	221369.2	177697.1	134459.7	94511.5	60430.0	34071.9
17	11-Nov-2031	263089.4	222348.2	179507.3	137225.7	98149.5	64601.5	38220.2
18	21-Nov-2031	263334.7	223078.8	180955.4	139509.9	101204.8	68155.5	41831.9
19	1-Dec-2031	263502.6	223672.7	182198.6	141508.2	103896.9	71304.6	45067.8
20	11-Dec-2031	263634.5	224205.0	183342.2	143353.8	106379.8	74207.4	48063.6
21	21-Dec-2031	263757.3	224722.6	184452.5	145132.3	108756.5	76975.2	50922.9
22	31-Dec-2031	263887.3	225253.9	185569.5	146897.1	111093.1	79683.1	53720.6
23	10-Jan-2032	264033.9	225814.4	186715.6	148679.2	113430.3	82379.7	56508.3
24	20-Jan-2032	264201.7	226411.5	187902.1	150495.5	115791.9	85095.6	59320.3
25	30-Jan-2032	264392.5	227047.6	189133.1	152353.7	118191.0	87848.9	62178.7
26	9-Feb-2032	0.0	227721.8	190408.6	154256.2	120633.5	90650.0	65097.5
27	19-Feb-2032	0.0	0.0	191726.2	156202.4	123121.5	93503.9	68084.6
28	29-Feb-2032	0.0	0.0	0.0	158189.9	125654.5	96412.7	71144.7
29	10-Mar-2032	0.0	0.0	0.0	0.0	128231.0	99376.8	74280.1
30	20-Mar-2032	0.0	0.0	0.0	0.0	0.0	102395.1	77491.3
31	30-Mar-2032	0.0	0.0	0.0	0.0	0.0	0.0	80778.5

Figure 13. This PCC provides m_{AA+} arrival mass values in kg for partial-rev, short-way turnaround abort cases from a nominal Leg-D transit. Cells with $m_{AA+} > m_i$ = 100000 kg are colored green in this PCC, while cells failing to meet this criterion are colored red and correspond to inviable abort cases. The boxed Cell B25 has maximum m_{AA+} in the PCC. Aborts from this dataset can be initiated as late as 3 August 2031, 60 days after nominal waypoint departure.

10.7 Abort Summary

Table 25 pulls together the six turnaround abort cases documented in the foregoing subsections, facilitating easy comparison of key parameters. All cases are performed contemporaneously with the Earth/Mars opposition at 04.497 May 2031 UTC.

Table 25. Documented for each abort case in the foregoing subsections are the nominal departure time t_D, nominal time-of-flight Δt, mass after abort triggers payload jettison m_{AT-}, and the time of latest turnaround (TLT) in days after nominal departure.

Abort Case	Nominal t_D (UTC)	Nominal Δt (d)	m_{AT-} (kg)	TLT (d after t_D)
Outbound Single-Leg	31.0 Dec 2030	285	341563	60
Leg-A	16.0 Dec 2030	145	294040	30
Leg-B	15.0 May 2031	150	481347	60
Return Single-Leg	06.0 Dec 2030	235	584675	90
Leg-C	01.0 Dec 2030	180	444046	30
Leg-D	04.0 Jun 2031	115	539428	60

Readers are advised to treat absolute viability dates in the foregoing abort scenarios with caution, as they are primarily intended for comparison between scenarios. These dates are heavily dependent on preliminary Starship capability data, and this vehicle has yet to fly in interplanetary space. As previously mentioned, unproven and unrestricted interchange between payload and propellant masses is assumed. Likewise, there is no demonstrated capability to jettison all payload mass, particularly on short notice. At best, viability dates provide semi-quantitative insight regarding degree of difficulty from one abort case to another with m_{AA+} as a metric.

In a heliocentric sense, it should be kept in mind that turnaround aborts do not "turnaround" at all. The Cell D9 Leg-D abort case from Figure 13's PCC serves as an example in Figure 14. Reference Figure 4 to view the entire Leg-C/D nominal trajectory leading to this abort scenario.

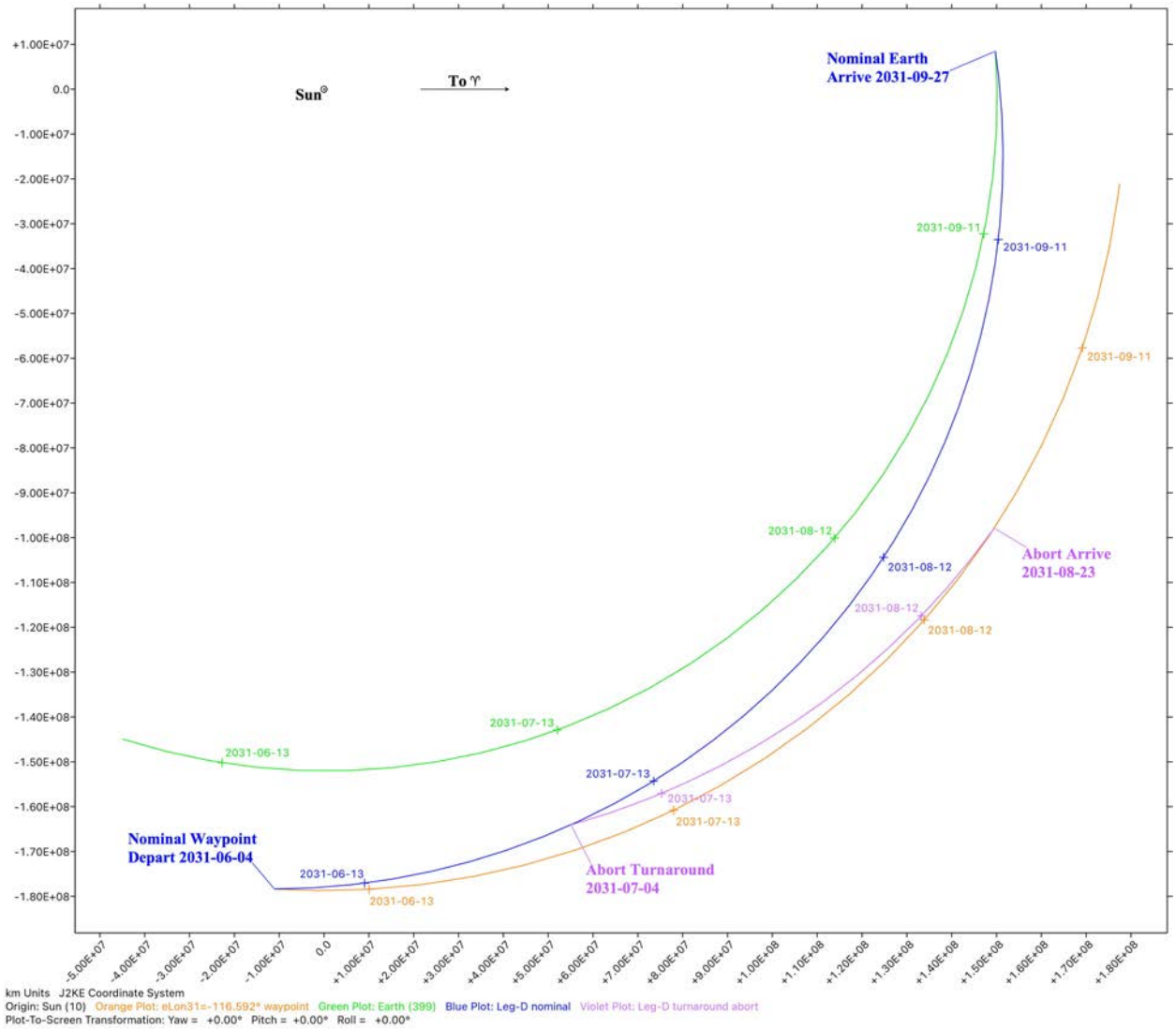

Figure 14. Inertial heliocentric ecliptic plane motion for Earth (green), waypoint (orange), nominal Leg-D (blue), and a Leg-D turnaround abort example from Figure 13, Cell D9 (violet) is plotted. This abort is initiated 30 days after nominal waypoint departure. Time ticks ("+" markers) are annotated with 00:00 UTC dates in YYYY-MM-DD format at 30-day intervals. The direction annotated "To ♈" points along zero ecliptic longitude λ.

11.0 Future Synodic Waypoints Research

Initial waypoint ecliptic longitudes λ_{31}, λ_{33}, λ_{31r}, and λ_{33r} computed in Sections 5.0 and 6.0 are each a product of 2LL scans confined to six-month periods ending near Table 1's 2031 or 2033 Earth/Mars opposition dates. These have served to demonstrate all four waypoints thus initialized will support viable Earth/Mars transits over the 15 years spanned by Table 1 dates. How might these locally optimized λ values change if their 2LL scans instead spanned the entire 15-year Table 1 interval? This is low-hanging fruit for future analysis.

As Earth/Mars transport technology and economics become more refined, assumptions made in this paper will require revision. For example, the 5-day minimum waypoint loiter time Δt_{Lmin}, initially assumed in Section 5.0, may need to be increased. And, as noted in Subsection 10.7, the interchangeability of Starship propellant mass m_P and payload mass m_Y, together with capability to jettison m_Y, are currently unknown. Indeed, an interplanetary transport significantly different from vintage 2024 Starship design may be the first to utilize Earth/Mars waypoints.

As new capabilities such as the NEO Surveyor space telescope[18] and Vera C. Rubin observatory[19] become operational, the rate of NEO discoveries is expected to increase significantly. Therefore, scans of the SBDB for natural Earth/Mars waypoint candidates and proximal resources, akin to that documented in Section 7.0, should be conducted regularly. When a NEO with semi-major axis near the ideal 1.195 AU is predicted to drift into proximity with an ecliptic longitude supporting waypoint utilization, resources required to bring about this support should be estimated for serious consideration. Applying these resources could entail correcting the NEO orbit for protracted waypoint service or transport of useful material from the NEO to a proximal existing waypoint.

The $j = 2$ synodic resonance waypoint orbit developed in Section 3 for Earth/Mars transport can also be applied to Venus/Earth logistics. Because the heliocentric orbit eccentricity of Venus is 0.0068 [2, Table 15.6, p. 704], even less than Earth's orbit, variations in the time between successive oppositions found in Table 1 for Earth and Mars will be greatly reduced for Earth and Venus. Although the Earth-concentric waypoint orbits developed in this paper are far from concentric with the orbit of Mars, a similar waypoint orbit placed between Earth and Venus will be highly concentric with the orbits of both planets. This geometry will render propulsive requirements and transit times highly repeatable from one Venus/Earth opposition to another.

Recall Section 8.0 has demonstrated increased payload mass is deliverable to more destinations via waypoints than with a single-leg Earth/Mars transit. Is there an analog between this finding and terrestrial transport? Personal experience with booking transcontinental U.S. air travel and tracking long-haul package deliveries indicates nonstop routing in these contexts is rare with respect to multi-stop itineraries. Presumably, nonstop transcontinental transport is less profitable than staged alternatives, but no authoritative and comprehensive data confirming this hypothesis have been found in the public domain other than circumstantial information documented in the Appendix. Until authoritative and comprehensive data are obtained, analogies between economies of Earth/Mars transport via waypoints and those of long-haul terrestrial transportation remain unsubstantiated.

12.0 Conclusions

This paper has introduced the concept of interplanetary waypoints in low-eccentricity heliocentric orbits concentric/coplanar with Earth's and positioned 19.5% farther from the Sun. These orbits have a synodic period with Earth exactly twice that of Mars with Earth. In such an orbit, a waypoint occupies nearly the same position leading or trailing the Sun/Earth/Mars line every other Earth/Mars opposition, an interval averaging 4.27 years. Four values for this

[18] Reference https://neos.arizona.edu (accessed 15 April 2024).
[19] Reference https://rubinobservatory.org (accessed 15 April 2024).

position have been determined such that either of two outbound waypoints and either of two return waypoints are well situated every Earth/Mars transit opportunity. Each waypoint can then become infrastructure at which consumables may be replenished and payload may be exchanged as humans and cargo are transported between Earth and Mars. A waypoint is distinct from a cycler because it never crosses either planet's orbit and naturally supports half of outbound or return Earth/Mars transit opportunities without targeted orbit corrections.

Simulations conducted herein have shown interplanetary transits through a waypoint require more total propellant and slightly more time than do single-leg alternatives. When these simulations assume consumables are replenished at a waypoint, however, more payload mass can be transported between Earth and Mars over a 15-year synodic sequence than with contemporaneous single-leg transits.

At present, no known asteroid is in an orbit permitting it to serve regularly as an Earth/Mars waypoint. Even if imminent asteroid surveys fail to discover a natural waypoint, artificial ones can be established with essential habitat, life support, and communications gear transported from Earth to ideal orbits. Thereafter, radiation shielding, consumables, and other transport-enabling material from myriad accessible natural bodies can be gathered, refined, and cached at nascent waypoints.

During conjunction periods, when Mars is on the other side of the Sun from Earth, direct communications between the two planets is degraded or inoperable. All four waypoints developed for Earth/Mars transport by this paper have been shown to be well positioned for serving as "bent pipe" communications relays during any of these conjunctions.

A two-leg transit, by virtue of its planned waypoint stopover, doubles the available forward abort options and helps shorten the time to arrive at a haven compared to a single-leg transit's itinerary. Turnaround aborts, with their propulsive challenges, have been simulated for single-leg and two-leg transits. In both itineraries, a latest viable turnaround point is reached weeks after departure for the interplanetary transport capability assumed by this paper. The time from departure to this latest turnaround tends to be more protracted for single-leg than for two-leg transits. Many late turnaround aborts are likely of low value, however, because they arrive back at the departure point *after* a forward abort would have arrived at the nominal destination.

Single-leg Earth/Mars transits are the baseline to which this paper's two-leg waypoint-enabled concept is naturally compared. Much of the data presented herein facilitates concise comparisons along these lines, and they are summarized in Table 26.

Table 26. Comparisons between conventional single-leg Earth/Mars transits and two-leg transits through an intermediate waypoint are summarized. "Min $\sum v_\infty$" transits are equivalent to those requiring minimal propulsion. Reference Tables 20/21 for associated transit times and deliverable payload masses. These masses reflect interplanetary transport-specific performance assumptions intended to facilitate comparison between the two transit itineraries and are not comprehensive values. Section 9.0 details Earth/Mars communications support offered by waypoints, and Table 25 contains limited transit abort capability data. Gray shading indicates an attribute is not applicable to single-leg transits.

Attribute	Single-Leg Transits	Two-Leg Transits
Min $\sum v_\infty$ transit time to waypoint		115-180 days
Min $\sum v_\infty$ transit time to Mars	200-290 days	300 days
Min $\sum v_\infty$ transit time to Earth	195-300 days	300 days
Payload mass to waypoint		96468-286771 kg
Payload mass to Mars	142566-179238 kg	63817-351466 kg
Payload mass to Earth	136992-178882 kg	112222-217104 kg
Solar conjunction comm relay	None	Every conjunction
Latest turnaround abort to Earth	60 days	30 days
Latest turnaround abort to Mars	90 days	30 days
Latest turnaround abort to waypoint		60 days

Acknowledgment

The author was originally inspired to develop this interplanetary waypoint concept while attending a Keck Institute for Space Studies (KISS) function titled "Applications of Asteroid Redirection Technology Workshop" and held at the California Institute of Technology April 7-9, 2014.[20] After nearly a decade of research, followed by dedicated software development of the Two-Leg Lambert processor in December 2023, comprehensive documentation of this idea has been produced here for initial publication.

Also in attendance at the KISS workshop was Dr. Michele Gates. She was among the first with whom the author discussed synodic-resonant waypoints in an Earth/Mars transport context. A decade later, Dr. Gates was the first to review and comment on this paper. Her extensive feedback is greatly appreciated.

[20] Reference https://www.kiss.caltech.edu/workshops/asteroid/asteroid3.html (accessed 6 March 2024).

References

[1] C. S. Rall, "Free-Fall Periodic Orbits Connecting Earth and Mars", TE-34, Massachusetts Institute of Technology, 1969.[21]

[2] P. K. Seidelmann (ed.), *Explanatory Supplement to the Astronomical Almanac*, University Science Books, Sausalito, CA, 1992.

[3] J. D. Giorgini, D. K. Yeomans, A. B. Chamberlin, P. W. Chodas, R. A. Jacobson, M. S. Keesey, J. H. Lieske, S. J. Ostro, E. M. Standish, R. N. Wimberly, "JPL's On-Line Solar System Data Service", *Bulletin of the American Astronomical Society*, Vol. 28, No. 3, p. 1158, 1996.[22]

[4] B. S. Borisov, "Three-Planet Resonances in the Solar System", *Bulgarian Astronomical Journal*, Volume 18-1, Bulgarian Academy of Sciences, 2012.[23]

[5] B. W. Barbee, P. A. Abell, D. R. Adamo, C. M. Alberding, D. D. Mazanek, L. N. Johnson, D. K. Yeomans, P. W. Chodas, A. B. Chanberlin, V. P. Friedensen, "The Near-Earth Object Human Space Flight Accessible Targets Study: An Ongoing Effort to Identify Near-Earth Asteroid Destinations for Human Explorers", 2013 IAA Planetary Defense Conference, Flagstaff, AZ, April 15-19, 2013.[24]

[6] A. E. Turner, "Deep Space Relay To Support Communications Between Earth And Mars", AAS 17-218, *Spaceflight Mechanics 2017: Proceedings of the 27th AAS/AIAA Space Flight Mechanics Meeting Held February 5-9, 2017, San Antonio, Texas, U.S.A*.

[21] This PhD thesis may be downloaded at https://ntrs.nasa.gov/api/citations/19700017824/downloads/19700017824.pdf (accessed 3 December 2023).

[22] Available at http://ssd.jpl.nasa.gov/?horizons (accessed 4 December 2023), the service is informally cited as *Horizons* throughout this paper.

[23] This paper may be downloaded at https://www.astro.bas.bg/AIJ/issues/n181/9-BBorisov.pdf (accessed 4 March 2024).

[24] A PDF of this presentation can be downloaded at https://iaaspace.org/wp-content/uploads/iaa/Scientific%20Activity/conf/pdc2013/IAA-PDC13-04-13pr.pdf (accessed 5 January 2024).

Appendix

Section 8 has demonstrated two-leg Earth/Mars transits utilizing intermediate waypoints can transport significantly more payload mass to more destinations than contemporaneous single-leg transits. Is a similar payoff in operation for long-haul U.S. air transport? This appendix documents statistics demonstrating nonstop flights between East Coast and West Coast airports in the contiguous U.S. are but a small fraction of all itineraries bookable through websites provided by the four most patronized U.S. airlines. In order of decreasing numbers of passengers carried in a year, these are American Airlines, Delta Air Lines, Southwest Airlines, and United Airlines.[25]

Consulting a list of the busiest U.S. airports, with the busiest ranked #1,[26] the four highest ranked on the East Coast served by all four of the most patronized airlines are #1 Hartsfield-Jackson Atlanta International Airport (ATL), #8 Orlando International Airport (MCO), #9 Miami International Airport (MIA), and #16 Logan International Airport (BOS). The four highest ranked West Coast airports served by all four airlines are #5 Los Angeles International Airport (LAX), #11 Seattle-Tacoma International Airport (SEA), #14 San Francisco International Airport (SFO), and #33 Portland International Airport (PDX).

During the week starting 2 June 2024, the four airlines' respective websites are then polled for transcontinental flights between the selected airports while the number of nonstop flights N and other flights O for each airline are tallied over the 7-day interval from one airport to the other four on the opposite coast. It should be understood these *bookable transcontinental itineraries* (BTIs) are but a subset of all transcontinental flights one could purchase during the specified week. Itineraries utilizing multiple airlines are excluded, and some websites appear to limit options (for example, American never lists more than 40 BTIs between two airports on a specified day).

If nonstop BTIs are available between specific airports on a specific day, each airline's website always lists them first. Thus, any excluded flight options would be multi-stop, and the $N/(N + O)$ quotient would be inflated. With the foregoing caveats in mind, consider the Table 27 data.

Table 27. Sequenced by departing airport, BTIs for the week beginning 2 June 2024 are decomposed according to "nonstop" and "other" tallies.

Departing Airport	N (nonstop BTIs)	O (other BTIs)	$N/(N + O)$
ATL	224	3529	6.0%
MCO	90	3510	2.5%
MIA	99	3268	2.9%
BOS	158	4021	3.8%
LAX	268	3868	6.5%
SEA	118	3226	3.5%
SFO	161	3104	4.9%
PDX	36	3367	1.1%

[25] Reference https://en.wikipedia.org/wiki/List_of_largest_airlines_in_North_America (accessed 1 May 2024).
[26] Reference https://en.wikipedia.org/wiki/List_of_the_busiest_airports_in_the_United_States (accessed 4 May 2024).

Among all BTIs tallied in Table 27 and numbering 29047, only 1154 or 4.0% are nonstop. Despite the convenience and reduced costs associated with nonstop transcontinental air travel, such flights are but a small fraction of all options available to transcontinental passengers. Factors driving major airlines toward this routing strategy must be profit-motivated, or these businesses would have failed over the decades they have operated. Rationale favoring multi-stop BTIs is obscure and likely confined to proprietary airline business plans. Nevertheless, the economics behind multi-stop BTIs is hypothesized to have an interplanetary transport analog that will compel establishment and regular use of strategically placed waypoints orbiting the Sun between planets.